



# Optimal probabilistic design of multi-band power system stabilizers using the two-point estimate method

Wesley Peres<sup>1</sup>

Received: 14 January 2024 / Accepted: 14 August 2024

© The Author(s), under exclusive licence to Springer-Verlag GmbH Germany, part of Springer Nature 2024

## Abstract

This paper introduces an optimization approach for the probabilistic design of multi-band power system stabilizers, considering demand uncertainties. The primary objective is to minimize the sum of central gains for each multi-band structure. The approach incorporates inequality constraints to manage parameter bounds and to ensure the probabilities of achieving security (based on the minimum damping ratio) and stability (based on the spectral abscissa). To address this complex problem, particle swarm optimization is proposed in conjunction with the two-point estimate method (2PEM) for probabilistic small-signal analysis. The 2PEM facilitates the use of a limited set of samples, enhancing efficiency. The efficacy of this approach is demonstrated through results obtained for a Brazilian test system and the New England test system, validated using Monte Carlo simulation. These results confirm both the accuracy and computational efficiency of the proposed method. Additionally, time-domain nonlinear simulations affirm the system's stability under large perturbations.

**Keywords** Multi-band power system stabilizers (MB-PSS) · Probabilistic tuning · Two-point estimate method (2PEM) · Monte Carlo simulation · Uncertainty

## Abbreviations

2PEM	Two-point estimate method
BA	Bat algorithm
CCA	Cooperative coevolutionary algorithm
CPOD	Conventional power oscillation damper
CPSS	Conventional power system stabilizer
CS	Cuckoo search
DBA	Directional bat algorithm
DE	Differential evolution

---

✉ Wesley Peres  
wesley.peres@ufsj.edu.br

<sup>1</sup> Department of Electrical Engineering, Federal University of São João del-Rei - UFSJ, São João del-Rei, Brazil

D-SSSA	Deterministic small-signal stability assessment
ESS	Energy storage system
FACTS	Flexible AC transmission systems
FFOA	Fruit fly optimization algorithm
FO	Firefly optimization
GA	Genetic algorithm
LFO	Low-frequency oscillations
LHS	Latin hypercube sampling
MB-POD	Multi-band power oscillation damper
MB-PSS	Multi-band power system stabilizer
MCS	Monte Carlo simulation
MICA	Modified imperialist competitive algorithm
MRAC	Model reference-based adaptive control
PDF	Probability density functions
PSO	Particle swarm optimization
P-SSSA	Probabilistic small-signal stability assessment
SG	Synchronous generator
SSSA	Small-signal stability assessment
STATCOM	Static synchronous compensators
VSC-HVDC	Voltage source converters based high voltage direct current systems
WADC	Wide area damping controller
WAMS	Wide area measurement systems
WG	Wind generator

## 1 Introduction

### 1.1 Motivation

Angular Small-Signal Stability Assessment (SSSA) studies Low-Frequency Oscillations (LFO) that emerge from unbalanced torques in synchronous generators following minor perturbations such as load and generation changes. These oscillations can reduce the capacity to transfer power between areas, potentially leading to blackouts [1]. Various control structures can mitigate LFO.

The first is Conventional Power System Stabilizers (CPSS), implemented in synchronous generators to introduce a damping torque component through modulation of the excitation voltage [2–4]. CPSS, comprising stages of gain, washout filter, and lead lag blocks, are effective in damping local modes (1–2 Hz) and can damp inter-area modes (0.1–1 Hz) with coordinated design [5].

However, the coordinated design of multiple CPSS can be impaired by market issues [6], and therefore conventional power oscillation dampers (CPODs) fitted on Flexible AC Transmission Systems (FACTS) are a secondary strategy to damp the LFO through voltage or power modulation. In [7], the CPOD parameters in the static voltage compensators (SVC) are optimized using the Seeker optimization Algorithm.

The development of Wide-Area Measurement Systems (WAMS), providing phasor measurements, has enabled remote signals for LFO damping [8]. Remote signals enhance the observability of oscillation modes. Reference [6] presents a Linear Quadratic Regulator-based approach to design Wide Area Damping Controller (WADC) parameters, a central controller using remote WAMS signals for LFO damping. In [9] a method is proposed to identify the most effective input–output pairs for WADC to maximize oscillation mode damping, and [10] addresses tuning of WADC parameters to mitigate the impact of remote signal channel failures.

Introduced in the early 2000s for the Hydro-Québec system, Multi-Band Power System Stabilizers (MB-PSS) represent another control structure for LFO damping [11]. MB-PSS consists of three bands that target specific frequency ranges: low (0.01–0.1 Hz for global modes), intermediate (0.1–1 Hz for inter-area) and high frequency (1–10 Hz for local modes). Each band features differential filters with gain, lead-lag blocks, and a hybrid block, exhibiting symmetric gain around central frequencies and gain attenuation above 10 Hz to minimize issues such as PSS saturation and noise [12, 13].

Most of the CPSS, CPOD and MB-PSS model tuning methods rely on deterministic analysis, assuming known loads and renewable generation sources [14]. However, with increasing weather dependency and integration for decarbonization [15, 16], uncertainty levels in power systems are rising, necessitating controllers' design tools that can accommodate these uncertainties [17]. This requirement is particularly evident with the recently proposed MB-PSS, where most parameter design approaches remain deterministic.

## 1.2 Literature review

### 1.2.1 Multi-band power system stabilizer applications

MB-PSS was initially proposed for synchronous generators in the Hydro-Québec system in [11]. In [18], a heuristic technique focusing on central frequencies and gains was introduced. An extensive performance comparison between MB-PSS and the accelerating power-based PSS (PSS2B) is presented in [12]. In [19] an optimization approach, solved by differential evolution, is proposed for the design of the MB-PSS parameter, aiming to minimize the quadratic error of the angular speed. In [20] a combination of the culture Algorithm, particle swarm optimization, and coevolutionary Algorithm is suggested for the design of the MB-PSS parameters to minimize the integral of the absolute time-weighted error of the angular speed. The Steepest Descent Method for optimizing MB-PSS parameters is employed in [21]. A gradient-based nonlinear optimization algorithm for MB-PSS tuning is proposed in [22].

The Multi-Band Power Oscillation Damper (MB-POD) is introduced in [23] with the same structure as MB-PSS for installation in Static Synchronous Compensators (STATCOM) and SVC, enhancing voltage stability and LFO damping using Wide-Area Measurement Systems signals. An MB-PSS based on remote signals from

Wide-Area Measurement Systems for synchronous generators is proposed in [24]. A hybrid optimization algorithm combining the steepest descent method and the gravity search algorithm is presented in [25] to maximize the damping of LFO using MB-PSS.

In [26] a modified particle swarm optimization is suggested for the MB-PSS design by minimizing the integral of the time-weighted absolute error of the angular speed. An MB-POD is proposed to modulate the susceptance of SVC in [13] to maximize the damping of LFO. Adaptive control based on model reference (MRAC) for the MB-PSS design is introduced in [27]. An analytical pole placement approach is proposed using the Newton–Raphson method for the MB-PSS design in [28]. The role of MB-POD in STATCOM in improving primary frequency control in systems with high penetration of wind energy is investigated in [29]. The Interior Point Method is used in [30] to design the MB-POD parameters for STATCOM to damp the LFO. In [31], a hybridization of particle swarm optimization with pattern search is proposed for the MB-PSS design. The Mayfly Optimization Algorithm for designing MB-POD for SVC is suggested in [32]. Lastly, [33] presents an MRAC-based MB-POD for wind generators to damp the LFO. Table 1 summarizes the publications addressed here on the multiband control structure.

### 1.2.2 Designing power system stabilizers using probabilistic methods

The approaches for MB-PSS tuning, as described in Table 1, are deterministic, developed within the Deterministic Small Signal Stability Assessment (D-SSSA) framework. These approaches work assuming that the loads and generations from renewable sources are known to evaluate security and stability through modal analysis [4]. To meet the security requirement, it must be ensured that the minimum damping ratio in closed-loop operation is at least a certain level (for example, 10%, as suggested in [34]). The stability requirement is fulfilled by ensuring that all eigenvalues in closed-loop operation lie on the left side of the complex plane, determined by the spectral abscissa [4]. However, these assumptions may not always align with real-world scenarios, necessitating the application of Probabilistic SSSA (P-SSSA).

P-SSSA involves estimating the statistical values (means and standard deviations) of the output variables (minimum damping ratio and spectral abscissa) based on the means and standard deviations of input variables (loads and generations). In the literature, three types of methods are recognized to calculate these statistical variables for the outputs: (i) numerical, (ii) analytical, and (iii) approximate [17, 35].

Numerical methods for P-SSSA include, but are not limited to, Monte Carlo Simulation (MCS), Quasi-Monte Carlo Simulation (Quasi-MCS), and Latin Hypercube Sampling (LHS). MCS involves using a large set of probabilistically defined samples to calculate the statistical variables of the outputs. Although its results are considered benchmark, the method is computationally intensive. Applications of these numerical approaches for the assessment or design of conventional Power System Stabilizers (PSS) or Power Oscillation Dampers (POD) within the P-SSSA framework are proposed in various studies.

**Table 1** Publications regarding multi-band control structures

Year	Approach	Tuning approach	Controller	References
2000	Deterministic	–	MB-PSS SG	[11]
2003	Deterministic	Heuristic	MB-PSS SG	[18]
2005	Deterministic	Heuristic	MB-PSS SG	[12]
2012	Deterministic	Differential evolution	MB-PSS SG	[19]
2013	Deterministic	Culture Algorithm, Particle Swarm Optimization Coevolutionary Algorithm	MB-PSS SG	[20]
2013	Deterministic	Steepest Descent	MB-PSS SG	[21]
2015	Deterministic	Gradient	MB-PSS SG	[22]
2017	Deterministic	Gradient	MB-POD STATCOM MB-POD SVC	[23]
2018	Deterministic	Particle Swarm Optimization	MB-PSS SG	[24]
2018	Deterministic	Steepest Descent Method and Gravitational Search Algorithm	MB-PSS SG	[25]
2018	Deterministic	Particle Swarm Optimization	MB-PSS SG	[26]
2019	Deterministic	Particle Swarm Optimization	MB-POD SVC	[13]
2020	Deterministic	Model Reference-based Adaptive Control (MRAC)	MB-PSS SG	[27]
2020	Deterministic	Analytical Pole Placement using Newton–Raphson	MB-PSS SG	[28]
2020	Deterministic	Gradient	MB-POD STATCOM	[29]
2020	Deterministic	Interior Point Method	MB-POD STATCOM	[30]
2022	Deterministic	Particle Swarm Optimization and Pattern Search	MB-PSS SG	[31]
2023	Deterministic	Mayfly Optimization Algorithm	MB-POD SVC	[32]
2023	Deterministic	MRAC	MB-POD WG	[33]
2024	Probabilistic	Particle Swarm Optimization	MB-PSS SG	Proposed

In [36], Quasi-MCS is applied to evaluate P-SSSA systems with the integration of plug-in electric vehicles (PEVs). Detailed modeling of PEVs has been found to be required for a proper analysis. Simulations carried out for two-area 4-machine and New England 10-generator 39-bus systems indicated that the Quasi-MCS provided errors around 40% compared to the MCS (with a reduced set of samples, which provided errors ranging from 34 to 112%). In [37], the MCS is used to assess the P-SSSA of the IEEE 16-generator test system, considering three load levels (low, mid, high). The main goal is to generate a set of samples based on wind farm generation levels, calculate the Probability Density Function (PDF) of critical eigenvalues, and optimize the PSS parameters through the Genetic Algorithm. Another application of MCS is presented in [38]. It focuses on optimal probabilistic PSS tuning considering uncertainties in renewable energy and power load. Simulations conducted for the New England New York test system have shown that the deterministic framework tends to be too conservative because the solutions obtained for a particular operating state are assumed to remain satisfactory when the analysis extends

to other operating states. Finally, the LHS is integrated with the differential evolution method in [39] to design PSS for wind and synchronous generators, considering remote signals and uncertainties. The results for the two-area system and the New York and New England Interconnected Power Systems show 90% of reproducibility in a reduced computational time compared to the MCS.

Analytical methods such as the cumulative method, based on linearized models, offer results with reduced computational time. However, the process of linearization may introduce susceptibility to errors. Applications of these analytical methods in the P-SSSA context have been explored in various studies. In [14], it was demonstrated that the stochastic output of the wind farm deteriorates the probabilistic small-signal stability of power systems. To solve this problem, the authors proposed the coordinated design of power system stabilizers (PSS) and static VAR compensator damping controllers (SVC). The solution was obtained using a modified fruit fly optimization algorithm (MFOA) and the Cumulant method, and case studies were conducted for the two-area test system. In [40], an approach to maximize the probabilities of security and stability is proposed by using differential evolution for optimization and the Taylor series for probabilistic analysis. Simulations for the three-machine power system and the New England test system have shown that DE is not remarkably sensitive to its control parameters over specified ranges.

Gurung et al. proposed a series of works applying the Cumulant method to address uncertainties during controller design. The initial observation focuses on the reduced computational effort required to treat uncertainties (estimating the probabilities of security maximized during the design process). In [41], the Bat Algorithm is applied to design controllers for synchronous generators and wind generators, demonstrating its superiority over CS, FO, and PSO. In [42], a Directional Bat Algorithm is used to design controllers for synchronous generators, presenting better results than the conventional Bat Algorithm. Damping controllers for synchronous generators and Energy Storage Systems (ESS) were tuned in [43], showing the promising results of ESS in damping low-frequency oscillations. Finally, damping controllers for wind and solar generators were investigated in [44], indicating that the high penetration of photovoltaic systems can improve Probabilistic Small-Signal Stability when properly designed.

Approximate methods provide an effective balance between accuracy and computational efficiency. This is largely due to their reliance on a smaller, deterministically calculated set of data to estimate the statistical variables of the outputs. A notable example is the Two-Point Estimate Method (2PEM), introduced in [45]. The 2PEM simplifies the estimation process by replacing uncertain input variables with deterministic points strategically positioned on both sides of their mean values.

The first application of 2PEM in the P-SSSA context was presented in [46], where no design was carried out, and uncertainties in power loads were simulated for the 9-bus 3 generator system, showing a computational gain compared to MCS. Although no design was carried out, the uncertainties of wind speed and power load were addressed in [47]. Simulations with the New England 39-bus system demonstrated the effectiveness of 2PEM in assessing the P-SSSA compared to the MCS. In [48], the design and implementation of a probabilistic coordinated approach is

proposed for power systems with synchronous generators (SG), DFIGs, and FACTS devices. An optimization approach is formulated to maximize the probabilities of security and stability, and it is solved by employing a modified Imperialist Competitive Algorithm together with 2PEM (to perform the P-SSSA). The results of the modified 39-bus New England power system show the superiority of the proposed probabilistic approach over particle swarm optimization, the genetic algorithm, and the standard imperialist competitive algorithm.

Table 2 summarizes recent publications in the context of P-SSSA. As one can see, most P-SSSA applications consider conventional structures for PSS and POD.

### 1.3 Contributions

An examination of Tables 1 and 2 reveals a notable omission in the literature: the probabilistic design of MB-PSS has not been extensively explored. This paper aims to address this gap with the following contributions.

- The development of an optimization approach aimed at minimizing the sum of gains of the MB-PSS in synchronous generators. This approach incorporates inequality constraints to ensure that the probabilities of meeting security (minimum damping ratio) and stability (spectral abscissa) requirements are at least equal to a predetermined confidence level.
- The application of PSO [51] is proposed for solving the optimization problem, where each individual in the PSO represents a potential solution comprising the

**Table 2** Publications on recent P-SSSA

Year	Probabilistic method	Optimal tuning?	Controller	References
2007	2PEM	Only assessment	–	[46]
2008	Taylor series	DE	CPSS SG	[40]
2012	2PEM	Only assessment	CPSS SG	[47]
2013	Quasi-MCS	Only assessment	CPSS SG	[36]
2014	MCS	GA	CPSS SG	[37]
2015	Cumulant	FFOA	CPSS SG, CPOD SVC	[14]
2016	LHS	DE	CPSS SG, CPOD WG	[39]
2019	Cumulant	BA, CS, FO, PSO	CPSS SG, CPOD WG	[41]
2019	2PEM	MICA	CPSS SG, CPOD WG CPOD STATCOM	[48]
2020	Cumulant	DBA	CPSS SG	[42]
2020	Cumulant	FO	CPSS SG, CPOD ESS	[43]
2020	MCS	CCA	CPSS SG	[38]
2021	Cumulant	BA	CPOD WG, CPOD PV	[44]
2022	MCS	Only assessment	VSC-HVDC	[49]
2024	Series expansion	Only assessment	PSS-SG	[50]
2024	2PEM	PSO	MB-PSS SG	Proposed

central gains and frequencies of the MB-PSS in synchronous generators (SG). The evaluation of each individual is conducted within a P-SSSA framework, utilizing the 2PEM. This approach significantly reduces the computational burden associated with the assessment.

This is the first study to address the probabilistic design of MB-PSS employing the 2PEM. The results of the Southeastern Brazil and New England test systems [52] are validated using Monte Carlo simulations and time domain simulations.

## 1.4 Paper organization

This paper is structured as follows. Section 2 introduces preliminary concepts related to the MB-PSS model and the P-SSSA, utilizing both MCS and the 2PEM. Section 3 details the proposed probabilistic design methodology for MB-PSS, incorporating an optimization approach resolved using particle swarm optimization and 2PEM. Section 4 assesses the effectiveness of this approach using the Southeastern Brazil and New England test systems [52]. The conclusions drawn from this study are presented in Sect. 5. Additionally, Appendices A and B provide data on the test system and a deterministic approach for comparative purposes.

## 2 Preliminary concepts

### 2.1 Multi-band power system stabilizer

Figure 1 presents the simplified representation of the MB-PSS. It can be seen that the three bands are well separated with their central frequencies and central gains. Each band is associated with a specific oscillation mode: (i) low-frequency band for global modes (in red—0.01–0.1 Hz), (ii) intermediate-frequency band for inter-area modes (in green—0.1–1 Hz), and (iii) high-frequency band for local modes (in blue—1–10 Hz) [12, 18].

According to [18, 28], four tunable parameters define the structure depicted in Fig. 2:

1. central frequencies for low ( $F_L$ ), intermediate ( $F_I$ ), and high ( $F_H$ ) bands;
2. gains at central frequencies for low ( $K_L$ ), intermediate ( $K_I$ ), and high ( $K_H$ ) bands;
3. global gain ( $K_G$ ).

These parameters allow for the calculation of gains and time constants in Fig. 2 employing (1)–(5). These equations are associated with the low-frequency band and can be extended to other bands. The constant  $R$  is set to 1.2 and controls the bandwidth. Finally, the transducers in Fig. 3 obtain the signal required at the input of the MB-PSS ( $\Delta\omega_{L-I}$  and  $\Delta\omega_H$ ) [12].



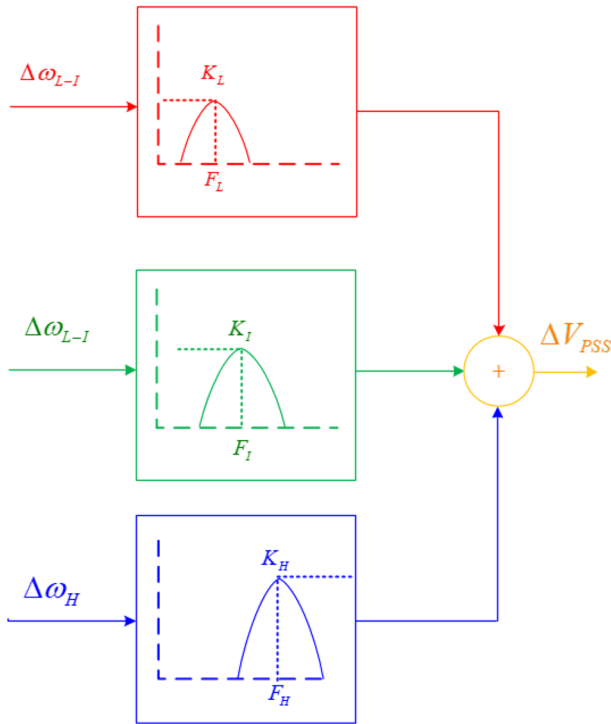


Fig. 1 Simplified representation of the MB-PSS

$$T_{L2} = T_{L7} = \frac{1}{2 \cdot \pi \cdot F_L \cdot \sqrt{R}} \quad (1)$$

$$T_{L1} = T_{L2} / R \quad (2)$$

$$T_{L8} = T_{L7} \cdot R \quad (3)$$

$$K_{L1} = K_{L2} = \frac{R^2 + R}{R^2 - 2R + 1} \quad (4)$$

$$K_{L11} = K_{L17} = 1 \quad (5)$$

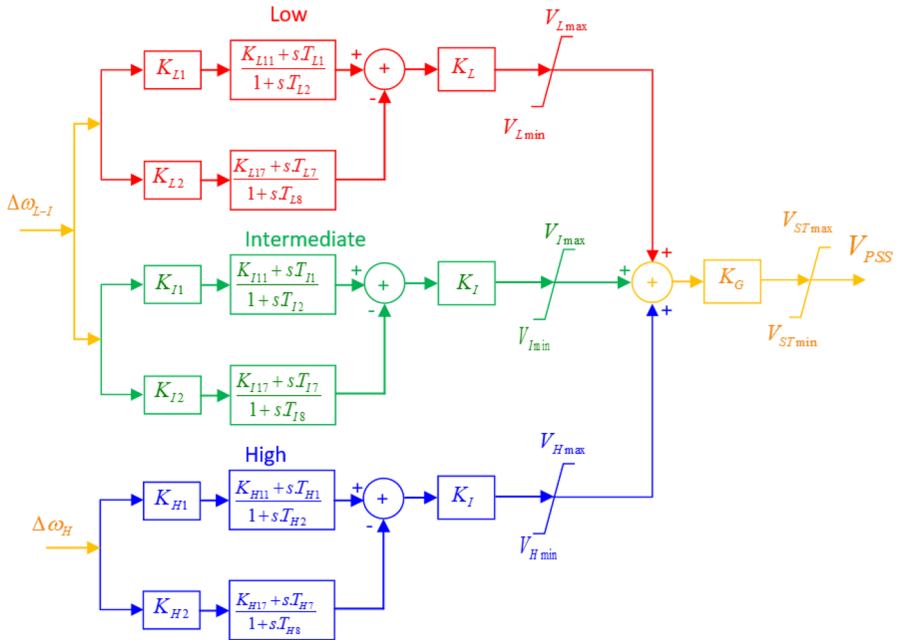


Fig. 2 Simplified structure of the MB-PSS

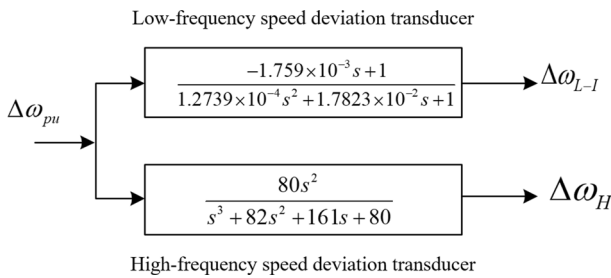


Fig. 3 High and low-frequency transducers of the MB-PSS

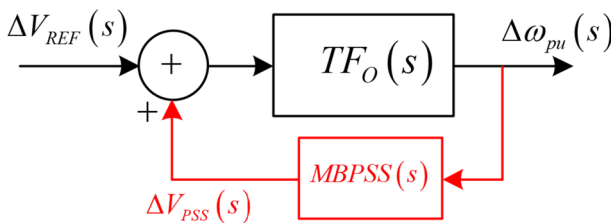


Fig. 4 Feedback procedure

## 2.2 Deterministic small signal stability analysis

Small signal stability analysis (SSSA) employs linearized equations to represent the dynamics of the power system. These equations are formulated in a state-space model [4] and are analyzed in two distinct operating modes: open-loop (without MB-PSS) and closed-loop (with MB-PSS). Equation (6) provides the state-space representation for the open-loop operation mode. Furthermore, the transfer function in the open-loop frequency domain ( $TF_O$ ) can be calculated as defined in Eq. (7) [53]. Figure 4 illustrates this transfer function and includes the transfer function for the Multi-Band Power System Stabilizer ( $MBPSS(s)$ ), calculated according to Figs. 2 and 3.

$$\begin{aligned}\Delta\dot{x} &= A_O\Delta x + B_O\Delta u \\ \Delta y &= C_O\Delta x\end{aligned}\quad (6)$$

where:

- $A_O$ ,  $B_O$ , and  $C_O$  are the state-space, input, and output matrices respectively;
- $\Delta x$  represents the vector of states composed of angular speeds, internal angles, internal voltages, and field voltages. Similarly,  $\Delta u$  denotes the vector containing input values, specifically  $\Delta V_{REF}$ , while  $\Delta y$  is the vector associated with output variables, in this case,  $\Delta\omega_{pu}$ .

$$TF_O(s) = C_O \cdot (sI - A_O)^{-1} \cdot B_O \quad (7)$$

The closed-loop state space representation, as shown in (8), is derived from a feedback representation depicted in Fig. 4. Similarly, a transfer function for the closed-loop operation is formulated and found in (9).

$$\begin{aligned}\Delta\dot{x} &= A_C\Delta x + B_C\Delta u \\ \Delta y &= C_C\Delta x\end{aligned}\quad (8)$$

where  $\Delta\dot{x}$  includes the state variable of MB-PSS.

$$TF_C(s) = C_C \cdot (sI - A_C)^{-1} \cdot B_C \quad (9)$$

From the closed-loop state space representation, it is possible to obtain  $m$  eigenvalues (from matrix  $A_C$  in (8)) or  $m$  roots from the denominator of  $TF_C(s)$ . For each pair of complex eigenvalues (or root) given in (10), it is possible to calculate a damping ratio according to (11).

$$\lambda_i = \sigma_i \pm j\omega_i \quad (10)$$

$$\xi_i = \frac{-\sigma_i}{\sqrt{\sigma_i^2 + \omega_i^2}} \quad (11)$$

Defining the minimum damping ratio and the spectral abscissa is essential to assess security and stability from the small-signal stability point of view. The minimum

damping ratio is the minimum value for all the calculated damping ratios. The spectral abscissa is the largest one of the real parts of the system's eigenvalues [54]. The system is stable when all  $\sigma_i$  are negative and  $\xi_i$  are positive [4]. The minimum damping ratio  $\xi_{\min}$  and the spectral abscissa  $\sigma_{\max}$  are calculated according to (12).

$$\begin{aligned}\sigma_{\max} &= \max(1, \dots, \sigma_i, \dots, \sigma_m) \\ \xi_{\min} &= \min(1, \dots, \xi_i, \dots, \xi_m)\end{aligned}\quad (12)$$

In power system operation, we say that the power system is secure when its minimum damping ratio  $\xi_{\min}$  is greater than or equal to a security level (10%, for example) [34]. The pseudocode used for the Deterministic Small Signal Stability Analysis is presented in Algorithm 1.

**Algorithm 1** Pseudocode for the Deterministic SSSA

- 
- 1: Read the power system data: loads.
  - 2: Read the power system data: topology, branch data, and dynamic parameters (generators and excitation systems).
  - 3: Read the power system data: parameters of each MB-PSS (central frequencies and gains).
  - 4: Solve the nonlinear power flow [55].
  - 5: Calculate the state-space equations given in (6) [4].
  - 6: Perform the feedback procedure depicted in Fig. 4 to obtain (8).
  - 7: Perform the modal analysis to calculate the eigenvalues of  $A_C$  [4, 53].
  - 8: Calculate the minimum damping ratio ( $\xi_{\min}$ ) and the spectral abscissa ( $\sigma_{\max}$ ) defined in (12).
  - 9: Evaluate the system small signal stability ( $\sigma_{\max} < 0$ ) and security ( $\xi_{\min} \geq 10\%$ ) [34].
- 

### 2.3 Probabilistic model of loads

In the probabilistic analysis performed in this paper, active and reactive power loads are random input variables  $X$  following a normal distribution as given in (13) [17]. The vector with mean values ( $X_{\text{mean}}$ ) and the covariance matrix ( $P_X$ ) are presented in (14).

$$X \sim N(X_{\text{mean}}, P_X) \quad (13)$$

where  $N$  denotes the normal distribution.

$$\begin{aligned}
 X_{\text{mean}} &= \begin{bmatrix} \mu_{P_{dk}} \\ \mu_{Q_{dk}} \end{bmatrix} \\
 P_X &= \begin{bmatrix} \sigma_{P_{dk}}^2 & 0 \\ 0 & \sigma_{Q_{dk}}^2 \end{bmatrix}
 \end{aligned}
 \tag{14}$$

where  $k = 1, \dots, nb$ .

Taking into account the  $nb$  load nodes, the dimensions of  $X_{\text{mean}}$  and  $P_X$  are  $(2nb \times 1)$  and  $(2nb \times 2nb)$ , respectively.

### 2.4 General formulation of the probabilistic small signal stability analysis

The probabilistic small-signal analysis in this paper can be seen as a multivariable nonlinear transformation given in (15), being the output vector  $Y$  composed of the minimum damping ratio ( $\xi_{\text{min}}$ ) and the spectral abscissa ( $\sigma_{\text{max}}$ ). In this case, the calculated mean vector ( $Y_{\text{mean}}$ ) and the covariance matrix ( $P_Y$ ) will be given as in (16).

$$Y = g(X) \tag{15}$$

The most widely used technique to solve (15) is Monte Carlo Simulation, whose pseudocode is given in Algorithm 2. It is based on a set of samples whose structure is depicted in Fig. 5.

$$\begin{aligned}
 Y_{\text{mean}} &= \begin{bmatrix} \mu_{\xi_{\text{min}}} \\ \mu_{\sigma_{\text{max}}} \end{bmatrix} \\
 P_Y &= \begin{bmatrix} \sigma_{\xi_{\text{min}}}^2 & 0 \\ 0 & \sigma_{\sigma_{\text{max}}}^2 \end{bmatrix}
 \end{aligned}
 \tag{16}$$

#### Algorithm 2 Pseudocode for the Probabilistic SSSA through the MCS

- 
- 1: Define the number of samples to be used in the MCS ( $n_{mcs}$ ). Each sample follows the structure defined in Fig. 5.
  - 2: **for all** samples  $i$  **do**
  - 3:     Generate a sample  $X_i$  following a normal distribution as given in (13).
  - 4:     Perform the deterministic SSSA for  $X_i$  for the calculation of the minimum damping ratio and the spectral abscissa: **Steps 1 to 8** of Algorithm 1.
  - 5:     Store  $\xi_{\text{min}}^i = \xi_{\text{min}}$  and  $\sigma_{\text{max}}^i = \sigma_{\text{max}}$ .
  - 6: **end for**
  - 7: Calculate  $\mu_{\xi_{\text{min}}}$  and  $\sigma_{\xi_{\text{min}}}$ .
  - 8: Calculate  $\mu_{\sigma_{\text{max}}}$  and  $\sigma_{\sigma_{\text{max}}}$ .
-

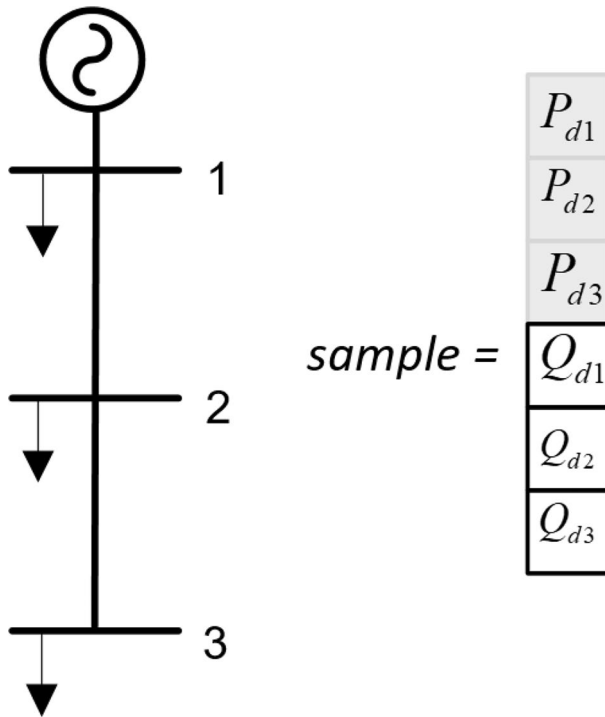


Fig. 5 Sample structure example for a system with 3 nodes

## 2.5 Probabilistic small signal stability analysis using the two-point estimate method—2PEM

A significant challenge with Monte Carlo simulation is the need for many samples to solve (15). An approximate method such as the Two Point Estimate Method (2PEM) is advantageous in alleviating the computational demand. The 2PEM simplifies the process by substituting uncertain input variables with deterministic points positioned on either side of their mean values. This approach enables the application of the deterministic procedure outlined in Algorithm 1. Consequently, the Deterministic SSSA, as discussed in Sect. 2.2, is executed twice for each uncertain variable: once using a value below the mean and then using a value above the mean, while maintaining other variables at their mean values. This section introduces the algorithm and the fundamental formulation of the 2PEM. Additional information and elaborations are available in [17, 56–58]. The pseudocode for the probabilistic SSSA using 2PEM is presented in Algorithm 3.

**Algorithm 3** Pseudocode for the Probabilistic SSSA through the 2PEM

- 1: Define the number of uncertain variables  $m = 2nb$  (number of active and reactive power loads) and the set  $k = 1 \dots m$ .
- 2: **for all**  $k \in m$  **do**
- 3: Determine the locations ( $\beta_{k,1}$  and  $\beta_{k,2}$ ) and the probabilities of concentrations ( $P_{k,1}$  and  $P_{k,2}$ ) as given in (17).

$$\begin{aligned} \beta_{k,1} &= \sqrt{m} \\ \beta_{k,2} &= -\sqrt{m} \\ P_{k,1} &= P_{k,2} = \frac{1}{2m} \end{aligned} \tag{17}$$

- 4: Determine the two concentrations for the variable  $k$  ( $x_{k,1}$  and  $x_{k,2}$ ) as given in (18). These points are positioned on either side of the mean value.

$$\begin{aligned} x_{k,1} &= \mu_{X,k} + \beta_{k,1}\sigma_{X,k} \\ x_{k,2} &= \mu_{X,k} + \beta_{k,2}\sigma_{X,k} \end{aligned} \tag{18}$$

- 5: Determine two samples for the input variable  $k$  as given in (19). Each sample represents a load vector as illustrated in Fig. 5.

$$\begin{aligned} X_1 &= [\mu_{X,1}, \mu_{X,2}, \dots, x_{k,1}, \dots, \mu_{X,m}]^T \\ X_2 &= [\mu_{X,1}, \mu_{X,2}, \dots, x_{k,2}, \dots, \mu_{X,m}]^T \end{aligned} \tag{19}$$

- 6: Perform the deterministic SSSA for  $X_1$  (the first sample for power loads): **Steps 1 to 8** of Algorithm 1.
- 7: Store  $\xi_{\min}^{k,1} = \xi_{\min}$  and  $\sigma_{\max}^{k,1} = \sigma_{\max}$ .
- 8: Perform the deterministic SSSA for  $X_2$  (the second sample for power loads): **Steps 1 to 8** of Algorithm 1.
- 9: Store  $\xi_{\min}^{k,2} = \xi_{\min}$  and  $\sigma_{\max}^{k,2} = \sigma_{\max}$ .
- 10: **end for**
- 11: Calculate the terms in (20).
- 12: Calculate  $\mu_{\xi_{\min}}$  and  $\sigma_{\xi_{\min}}$  as given in (21).
- 13: Calculate  $\mu_{\sigma_{\max}}$  and  $\sigma_{\sigma_{\max}}$  as given in (21).

$$\begin{aligned}
 E(\xi_{\min}) &= \sum_{k=1}^m \sum_{i=1}^2 (P_{k,i} \cdot \xi_{\min}^{k,i}) \\
 E((\xi_{\min})^2) &= \sum_{k=1}^m \sum_{i=1}^2 (P_{k,i} \cdot (\xi_{\min}^{k,i})^2) \\
 E(\sigma_{\max}) &= \sum_{k=1}^m \sum_{i=1}^2 (P_{k,i} \cdot \sigma_{\max}^{k,i}) \\
 E((\sigma_{\max})^2) &= \sum_{k=1}^m \sum_{i=1}^2 (P_{k,i} \cdot (\sigma_{\max}^{k,i})^2)
 \end{aligned} \tag{20}$$

$$\begin{aligned}
 \mu_{\xi_{\min}} &= E(\xi_{\min}) \\
 \sigma_{\xi_{\min}} &= \sqrt{E((\xi_{\min})^2) - \mu_{\xi_{\min}}^2} \\
 \mu_{\sigma_{\max}} &= E(\sigma_{\max}) \\
 \sigma_{\sigma_{\max}} &= \sqrt{E((\sigma_{\max})^2) - \mu_{\sigma_{\max}}^2}
 \end{aligned} \tag{21}$$

### 3 Proposed approach

Two critical aspects must be considered during the design of power system stabilizers. Firstly, the magnitude of the gains should not be large to prevent saturation of the output of the excitation system [54]. Secondly, it is imperative to address security and stability requirements in the presence of uncertainties. In such scenarios, the probabilities of meeting these requirements should be at least equal to a predetermined confidence level [14].

#### 3.1 Optimization problem

The proposed optimization approach is detailed in (22)–(25). Equation (22) describes the objective function, which is designed to minimize the sum of gains, thereby reducing the control effort. The probability of meeting the security requirement  $P_r\{\xi_{\min} \geq \xi_d\}$  must be at least 95%, as specified in (23). Equation (24) ensures that the probability of stability, indicated by the spectral abscissa  $P_r\{\sigma_{\max} < 0\}$ , is also at least 95%. Lastly, the optimization variables, as outlined in (26), are required to remain within the specified limits, as defined in (25) [59].



$$\min f(z) = \sum_{i=1}^{npss} (K_{Li} + K_{li} + K_{Hi} + K_{Gi}) \tag{22}$$

$$\text{s.t. } P_r \{ \xi_{\min} \geq \xi_d \} \geq 95\% \tag{23}$$

$$P_r \{ \sigma_{\max} < 0 \} \geq 95\% \tag{24}$$

$$z_i^{\min} \leq z_i \leq z_i^{\max} \tag{25}$$

where:

- $i = 1, \dots, npss$ , being  $npss$  the number of MB-PSS to be tuned. Each PSS follows the structure defined in Fig. 2.
- $\xi_d$  is the minimum damping ratio to ensure security (here,  $\xi_d = 10\%$ ).
- the probabilities are calculated based on the means and standard deviations defined in (16), according to [60].

$$z_i = [ K_{Li} \ K_{li} \ K_{Hi} \ K_{Gi} \ F_{Li} \ F_{li} \ F_{Hi} ] \tag{26}$$

### 3.2 Fitness function calculation

The optimization problem, as formulated in (22)–(25), presents complexities that make it challenging to solve using gradient-based methods. In contrast, population-based metaheuristic algorithms offer high-quality solutions in a reasonable computational time. In this context, the particle swarm optimization method [51] is used. Each individual in the PSO population  $ind_k$  is represented by a vector of dimension  $(1 \times 7npss)$ , which corresponds to a potential solution to the optimization problem, as depicted in (27). A fitness function,  $fit_k$ , is associated with each individual, as elaborated in (28).

$$ind_k = [ K_{Li} \ K_{li} \ K_{Hi} \ K_{Gi} \ F_{Li} \ F_{li} \ F_{Hi} ] \tag{27}$$

$$fit_k = \beta_1 \cdot F_1 + \beta_2 \cdot F_2 + \beta_3 \cdot F_3 \tag{28}$$

where,  $i = 1, \dots, npss$ ,  $\beta_1 = 1$  and  $\beta_2 = \beta_3 = 10^2$ .

The fitness function in (28) comprises three components:  $F_1$ ,  $F_2$ , and  $F_3$ . The first term  $F_1$ , defined in (29), is associated with the objective function in (22). The

remaining terms,  $F_2$  and  $F_3$ , serve as penalties within the fitness function, applied when the security and stability requirements, as specified in (23)–(24), are not met. In this case,  $F_2$  and  $F_3$  are calculated in (30)–(31). In particular, these penalizations are included through empirically adjusted weights, denoted as  $\beta_i$ .

$$F_1 = \sum_{i=1}^{npss} (K_{Li} + K_{Ii} + K_{Hi} + K_{Gi}) \quad (29)$$

$$F_2 = \begin{cases} |penal_1| & \text{if } P_r\{\xi_{\min} \geq \xi_d\} < 95\% \\ 0 & \text{otherwise} \end{cases} \quad (30)$$

where  $penal_1 = 95\% - P_r\{\xi_{\min} \geq \xi_d\}$ .

$$F_3 = \begin{cases} |penal_2| & \text{if } P_r\{\sigma_{\max} < 0\} < 95\% \\ 0 & \text{otherwise} \end{cases} \quad (31)$$

where  $penal_2 = 95\% - P_r\{\sigma_{\max} < 0\}$ .

It is important to note that the constraint (25) is handled directly by the PSO method for constrained optimization. Finally, the pseudocode for the calculation of the fitness function is presented in Algorithm 4.

#### Algorithm 4 Pseudocode for the Fitness Calculation

- 
- 1: Read an individual vector  $ind_k$  defined in (27).
  - 2: Solve the probabilistic SSSA through the 2PEM as given in Algorithm 3.
  - 3: Calculate the probabilities of satisfying the security and stability requirements.
  - 4: Calculate the fitness function  $fit_k$  as given in (28).
  - 5: Return  $fit_k$ .
- 

### 3.3 Particle swarm optimization algorithm

The Particle Swarm Optimization method was proposed in [51] and mimics the process that birds perform while searching for food. Individuals move into the search space based on cognitive and social information. The cognitive factor is associated with the best experience of the individuals themselves, and the social factor is associated with the best experience of the population. In generation  $t$ , each particle (or individual) has the following:

- a velocity  $v_k^t$ ;
- a position  $ind_k^t$ , representing a possible solution;
- the information about the best position achieved by the individual itself ( $pbest_k$ ). It is associated with cognitive information.

The previous parameters ( $v_k^t$ ,  $ind_k^t$ , and  $pbest_k$ ) are vectors ( $1 \times 7npss$ ), and  $ind_k^t$  is defined in (27). Finally, the best position among all individuals is stored in  $gbest$  (social information). Equations (32)–(34) are used to update the individual’s positions during the generations (or iterations).

$$v_k^{t+1} = w^t v_k^t + c_1 r_1 (pbest_k - ind_k^t) + c_2 r_2 (gbest - ind_k^t) \tag{32}$$

$$w^t = w_{\max} - \left( \frac{w_{\max} - w_{\min}}{t_{\max}} \right) t \tag{33}$$

$$ind_k^{t+1} = ind_k^t + v_k^{t+1} \tag{34}$$

In PSO,  $c_1$  and  $c_2$  are the acceleration constants, both set to 2. The random numbers  $r_1$  and  $r_2$  contribute to the stochastic nature of the algorithm. The inertia constant  $w^t$ , crucial for the balance of global and local search during the optimization process, varies at each generation  $t$ . It decreases from a maximum  $w_{\max} = 0.9$  to a minimum  $w_{\min} = 0.4$ , as defined in (33), with  $t_{\max}$  being the specified maximum number of generations.

The search space limits are defined in (35), associated with the constraints in (25). The velocities  $v_i^t$  are limited to 10% of the maximum values of (35), as given in (36). In cases where the limits set in (35)–(36) are violated, the variable is adjusted to the violated limit (feasibility test).

$$\begin{aligned} ind_k^{min} &= z^{min} \\ ind_k^{max} &= z^{max} \end{aligned} \tag{35}$$

$$-0.10 \times ind_k^{max} \leq v_k^t \leq 0.10 \times ind_k^{max} \tag{36}$$

The pseudocode for particle swarm optimization is presented in Algorithm 5.

**Algorithm 5** Pseudocode for Particle Swarm Optimization

- 
- 1: Define the objective function and the problem variables and initialize the algorithm parameters.
  - 2: Initialize iteration counter:  $t = 0$  and define  $t_{max}$ .
  - 3: Initialize the positions  $ind_k^t$  and velocities  $v_k^t$  of all particles within the permitted limits.
  - 4: Calculate the fitness function  $fit_k^t$  associated with each particle using the Algorithm 4.
  - 5: For all particles do:  $pbest_k = ind_k^t$  and set its fitness function  $f_{pbest_k} = fit_k^t$ .
  - 6: Find the best global position  $gbest$  and its fitness function  $f_{gbest}$  (the lowest value).
  - 7: **while**  $t \leq t_{max}$  **do**
  - 8:     **for all** particles  $k$  **do**
  - 9:         Calculate the inertia constant  $w^t$  using (33).
  - 10:         Update the velocity  $v_k^{t+1}$  using (32) and test the feasibility.
  - 11:         Update the position  $ind_k^{t+1}$  using (34) and test the feasibility.
  - 12:         Calculate the fitness function  $fit_k^{t+1}$  associated with the particle  $ind_k^{t+1}$  using the Algorithm 4.
  - 13:         **if**  $fit_k^{t+1} \leq f_{pbest_k}$  **then**
  - 14:             Set  $pbest_k = ind_k^{t+1}$  and  $f_{pbest_k} = fit_k^{t+1}$ .
  - 15:         **end if**
  - 16:     **end for**
  - 17:     Find the best global position  $gbest$  and its fitness function  $f_{gbest}$  (the lowest value).
  - 18:      $t = t + 1$ .
  - 19: **end while**
  - 20: **return**  $gbest$
- 

**3.4 Tutorial example****3.4.1 Flowchart**

The flowchart of the PSO method, detailed in Algorithm 5, is illustrated in Fig. 6. The Probabilistic Small Signal Stability Analysis (considering load uncertainties following a Normal Distribution) is conducted in **Steps 5** and **6** during the fitness function calculation.

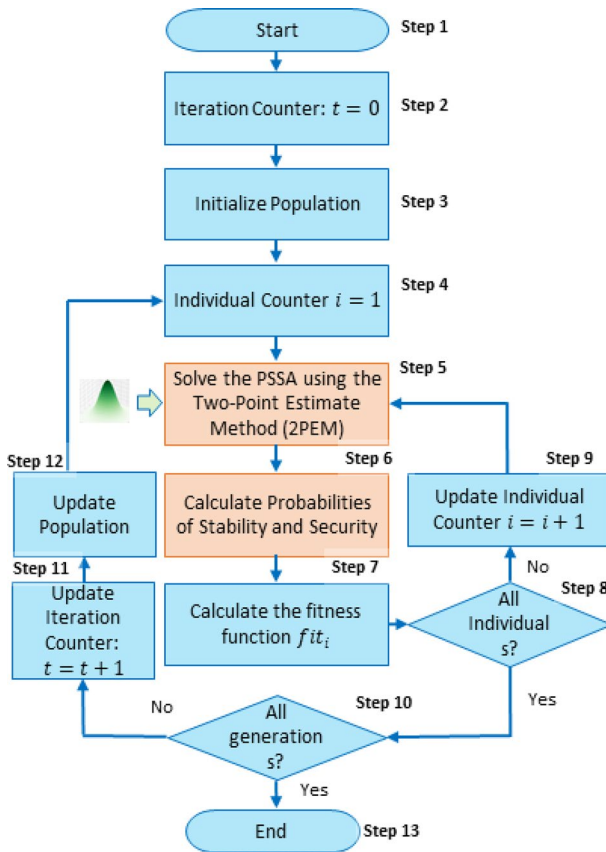


Fig. 6 Flowchart—optimization approach

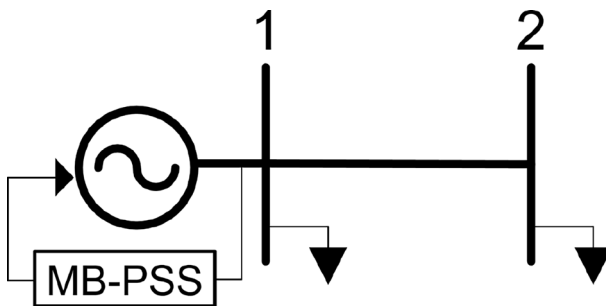


Fig. 7 Tutorial example

### 3.4.2 Example

Consider a tutorial power system with 2 nodes and one generator, as illustrated in Fig. 7. Probabilistic small signal stability analysis (**Step 5** of Fig. 6) follows the Algorithm 3.

(a) power loads follow the normal distribution as defined in (37):

$$\begin{aligned}
 P_{d1} &\sim N(\mu_{P_{d1}}, \sigma_{P_{d1}}) \\
 P_{d2} &\sim N(\mu_{P_{d2}}, \sigma_{P_{d2}}) \\
 Q_{d1} &\sim N(\mu_{Q_{d1}}, \sigma_{Q_{d1}}) \\
 Q_{d2} &\sim N(\mu_{Q_{d2}}, \sigma_{Q_{d2}})
 \end{aligned} \tag{37}$$

As defined in (38), the mean values are the nominal power loads given in  $X_{\text{mean}}$ . The covariance matrix is denoted as  $P_X$ .

$$\begin{aligned}
 X_{\text{mean}} &= \begin{bmatrix} \mu_{P_{d1}} \\ \mu_{P_{d2}} \\ \mu_{Q_{d1}} \\ \mu_{Q_{d2}} \end{bmatrix} = \begin{bmatrix} P_{d1}^{\text{nom}} \\ P_{d2}^{\text{nom}} \\ Q_{d1}^{\text{nom}} \\ Q_{d2}^{\text{nom}} \end{bmatrix} \\
 P_X &= \begin{bmatrix} \sigma_{P_{d1}}^2 & 0 & 0 & 0 \\ 0 & \sigma_{P_{d2}}^2 & 0 & 0 \\ 0 & 0 & \sigma_{Q_{d1}}^2 & 0 \\ 0 & 0 & 0 & \sigma_{Q_{d2}}^2 \end{bmatrix}
 \end{aligned} \tag{38}$$

- (b) The number of uncertain variables is  $m = 4$ .  
 (c) Calculate the locations and probabilities of concentrations. For each variable  $k$  ( $k = 1, \dots, 4$ ), two locations ( $\beta_{k,1}$  and  $\beta_{k,2}$ ) are calculated as given in (39). Similarly, the probabilities of concentrations ( $P_{k,1}$  and  $P_{k,2}$ ) are calculated in (40).

$$\begin{aligned}
 \beta_{1,1} &= \sqrt{m} = \sqrt{4} = 2 \\
 \beta_{1,2} &= -\sqrt{m} = -\sqrt{4} = -2 \\
 \beta_{2,1} &= \sqrt{m} = \sqrt{4} = 2 \\
 \beta_{2,2} &= -\sqrt{m} = -\sqrt{4} = -2 \\
 \beta_{3,1} &= \sqrt{m} = \sqrt{4} = 2 \\
 \beta_{3,2} &= -\sqrt{m} = -\sqrt{4} = -2 \\
 \beta_{4,1} &= \sqrt{m} = \sqrt{4} = 2 \\
 \beta_{4,2} &= -\sqrt{m} = -\sqrt{4} = -2
 \end{aligned} \tag{39}$$

$$\begin{aligned}
 P_{1,1} &= P_{1,2} = \frac{1}{2m} = \frac{1}{8} \\
 P_{2,1} &= P_{2,2} = \frac{1}{2m} = \frac{1}{8} \\
 P_{3,1} &= P_{3,2} = \frac{1}{2m} = \frac{1}{8} \\
 P_{4,1} &= P_{4,2} = \frac{1}{2m} = \frac{1}{8}
 \end{aligned}
 \tag{40}$$

(d) Two concentrations are calculated for each variable  $k$  as given in (41).

$$\begin{aligned}
 x_{1,1} &= \mu_{P_{d1}} + \beta_{1,1}\sigma_{P_{d1}} = \mu_{P_{d1}} + 2\sigma_{P_{d1}} \\
 x_{1,2} &= \mu_{P_{d1}} + \beta_{1,2}\sigma_{P_{d1}} = \mu_{P_{d1}} - 2\sigma_{P_{d1}} \\
 x_{2,1} &= \mu_{P_{d2}} + \beta_{2,1}\sigma_{P_{d2}} = \mu_{P_{d2}} + 2\sigma_{P_{d2}} \\
 x_{2,2} &= \mu_{P_{d2}} + \beta_{2,2}\sigma_{P_{d2}} = \mu_{P_{d2}} - 2\sigma_{P_{d2}} \\
 x_{3,1} &= \mu_{Q_{d1}} + \beta_{3,1}\sigma_{Q_{d1}} = \mu_{Q_{d1}} + 2\sigma_{Q_{d1}} \\
 x_{3,2} &= \mu_{Q_{d1}} + \beta_{3,2}\sigma_{Q_{d1}} = \mu_{Q_{d1}} - 2\sigma_{Q_{d1}} \\
 x_{4,1} &= \mu_{Q_{d2}} + \beta_{4,1}\sigma_{Q_{d2}} = \mu_{Q_{d2}} + 2\sigma_{Q_{d2}} \\
 x_{4,2} &= \mu_{Q_{d2}} + \beta_{4,2}\sigma_{Q_{d3}} = \mu_{Q_{d2}} - 2\sigma_{Q_{d3}}
 \end{aligned}
 \tag{41}$$

(e) Two samples are defined for each variable  $k$ , and two deterministic SSSA (Algorithm 1) are performed (for  $X_1$  and  $X_2$ ). Each sample is a vector of power loads. For each sample, the nonlinear power flow and the deterministic Small Signal Stability Analysis (considering a set of parameters for the MB-PSS) are conducted to calculate the associated minimum damping ratio ( $\xi_{min}$ ) and the spectral abscissa ( $\sigma_{max}$ ). This process is given in (42)–(45).

- $k = 1(P_{d1})$

$$[X_1 \ X_2] = \begin{bmatrix} x_{1,1} & x_{1,2} \\ P_{d2}^{nom} & P_{d2}^{nom} \\ Q_{d1}^{nom} & Q_{d1}^{nom} \\ Q_{d2}^{nom} & Q_{d2}^{nom} \end{bmatrix}
 \tag{42}$$

$$X_1 \rightarrow \xi_{min}^{1,1} = \xi_{min} \rightarrow \sigma_{max}^{1,1} = \sigma_{max}$$

$$X_2 \rightarrow \xi_{min}^{1,2} = \xi_{min} \rightarrow \sigma_{max}^{1,2} = \sigma_{max}$$

- $k = 2(P_{d2})$

$$[X_1 \ X_2] = \begin{bmatrix} P_{d1}^{nom} & P_{d1}^{nom} \\ x_{2,1} & x_{2,2} \\ Q_{d1}^{nom} & Q_{d1}^{nom} \\ Q_{d2}^{nom} & Q_{d2}^{nom} \end{bmatrix} \quad (43)$$

$$X_1 \rightarrow \xi_{\min}^{2,1} = \xi_{\min} \rightarrow \sigma_{\max}^{2,1} = \sigma_{\max}$$

$$X_2 \rightarrow \xi_{\min}^{2,2} = \xi_{\min} \rightarrow \sigma_{\max}^{2,2} = \sigma_{\max}$$

- $k = 3(Q_{d1})$

$$[X_1 \ X_2] = \begin{bmatrix} P_{d1}^{nom} & P_{d1}^{nom} \\ P_{d2}^{nom} & P_{d2}^{nom} \\ x_{3,1} & x_{3,2} \\ Q_{d2}^{nom} & Q_{d2}^{nom} \end{bmatrix} \quad (44)$$

$$X_1 \rightarrow \xi_{\min}^{3,1} = \xi_{\min} \rightarrow \sigma_{\max}^{3,1} = \sigma_{\max}$$

$$X_2 \rightarrow \xi_{\min}^{3,2} = \xi_{\min} \rightarrow \sigma_{\max}^{3,2} = \sigma_{\max}$$

- $k = 4(Q_{d2})$

$$[X_1 \ X_2] = \begin{bmatrix} P_{d1}^{nom} & P_{d1}^{nom} \\ P_{d2}^{nom} & P_{d2}^{nom} \\ Q_{d1}^{nom} & Q_{d1}^{nom} \\ x_{4,1} & x_{4,2} \end{bmatrix} \quad (45)$$

$$X_1 \rightarrow \xi_{\min}^{4,1} = \xi_{\min} \rightarrow \sigma_{\max}^{4,1} = \sigma_{\max}$$

$$X_2 \rightarrow \xi_{\min}^{4,2} = \xi_{\min} \rightarrow \sigma_{\max}^{4,2} = \sigma_{\max}$$

- (f) Calculation of the mean and standard deviation of damping ratio as given in (46)–(47).

$$E(\xi_{\min}) = \sum_{k=1}^4 \sum_{i=1}^2 (P_{k,i} \cdot \xi_{\min}^{k,i}) \quad (46)$$

$$E((\xi_{\min})^2) = \sum_{k=1}^4 \sum_{i=1}^2 (P_{k,i} \cdot (\xi_{\min}^{k,i})^2)$$

$$\begin{aligned} \mu_{\xi_{\min}} &= E(\xi_{\min}) \\ \sigma_{\xi_{\min}} &= \sqrt{E((\xi_{\min})^2) - \mu_{\xi_{\min}}^2} \end{aligned} \quad (47)$$

- (g) Calculation of the mean and standard deviation of spectral abscissa as given in (48)–(49).



$$E(\sigma_{\max}) = \sum_{k=1}^4 \sum_{i=1}^2 (P_{k,i} \cdot \sigma_{\max}^{k,i}) \tag{48}$$

$$E((\sigma_{\max})^2) = \sum_{k=1}^4 \sum_{i=1}^2 (P_{k,i} \cdot (\sigma_{\max}^{k,i})^2)$$

$$\mu_{\sigma_{\max}} = E(\sigma_{\max})$$

$$\sigma_{\sigma_{\max}} = \sqrt{E((\sigma_{\max})^2) - \mu_{\sigma_{\max}}^2} \tag{49}$$

The process defined in (37)–(49) is required to evaluate each PSO solution and is repeated several times during the optimization process. Its results are used to calculate the fitness function discussed in Sect. 3.2.

### 4 Results

The proposed approach is validated using two benchmark models from the literature [52]. The first model is the equivalent Brazilian 7-bus system, comprising 7 buses and 5 machines. The second model is the 39-bus New England test system, comprising 39 buses and 10 generators.

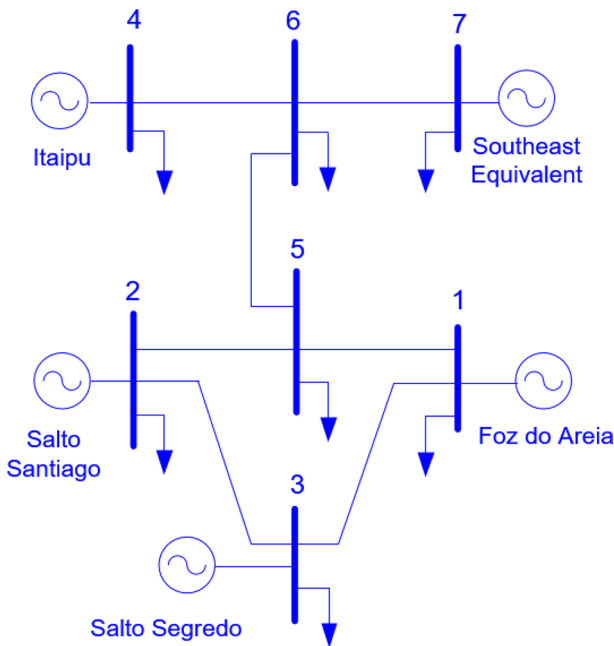


Fig. 8 South-Southeastern Brazil equivalent system

## 4.1 Equivalent model of the South-Southeastern Brazilian system

### 4.1.1 System description and optimization parameters

The test system utilized in this study is a seven-bus, five-machine configuration, as depicted in Fig. 8, where one machine represents the Southeastern Brazil system [52, 54, 61]. Detailed data on the power system are provided in Appendix 1. Synchronous generators are modeled using a third-order representation, while automatic voltage regulators are described using a first-order model.

It is noteworthy that this system is among the six benchmark systems recommended by the IEEE Task Force on Benchmark Systems for Stability Controls of the Power System Dynamic Performance Committee for analyzing and controlling electromechanical oscillations in power systems [52]. These benchmark systems were selected for their educational value and unique characteristics, which pose significant challenges in control system design relevant to the research community. Thus, utilizing this system in our paper is crucial as it is well-recognized and ensures reproducibility.

It should be noted that the performance of multiband power system stabilizers compared to conventional power system stabilizers, which are based on a classical structure, has been extensively studied in various works [12, 13, 25, 30]. However, this particular case study is exclusively focused on the MB-PSS structure.

Table 3 outlines the limits considered during the optimal adjustment of MB-PSS. Initially, the probabilistic design of MB-PSS, as detailed in Appendix 2, is conducted. Subsequently, the solution is validated using the probabilistic methods described in Algorithms 2 and 3. Following this, the proposed approach described in Sect. 3 is applied, and the controllers' performance is evaluated under different levels of uncertainty. Finally, angular transient stability is also analyzed.

Given seven load nodes, the total count of uncertainty input variables amounts to 14, which includes active and reactive power values. Consequently, for the probabilistic small signal analysis using 2PEM (using Algorithm 3), a total of 28 samples are required. In contrast, the MCS approach (outlined in Algorithm 2) will be implemented with 5000 samples. This study (MCS) will also include an analysis of convergence, specifically investigating the minimum number of samples required for the stabilization of the mean and standard deviation of the output variables.

**Table 3** Controller parameter boundaries [25]

Parameter	min	max
$F_L$ (Hz)	0.01	0.1
$F_I$ (Hz)	0.10	1.0
$F_H$ (Hz)	1.00	10.0
$K_L$ (pu)	0.01	30
$K_I$ (pu)	0.01	40
$K_H$ (pu)	0.01	120
$K_G$ (pu)	0.01	20

### 4.1.2 Deterministic design and probabilistic validation

The deterministic SSSA, conducted in open loop mode (without stabilizers), reveals system instability with a damping ratio of  $-12.224\%$ . Four MB-PSS units are installed in generators 1, 2, 3, and 4 to stabilize the system, as illustrated in Fig. 8. Generator 7, an equivalent system, is not equipped with an MB-PSS. The deterministic optimization process, detailed in Appendix 2, employs the following PSO parameters: 25 particles and 50 iterations. This results in 1250 fitness function evaluations ( $25 \times 50 = 1250$ ). Convergence is achieved in 48.48 s, with the evolution of the fitness function displayed in Fig. 9. The desired damping ratio is  $10\%$  ( $\xi_d = 10\%$ ).

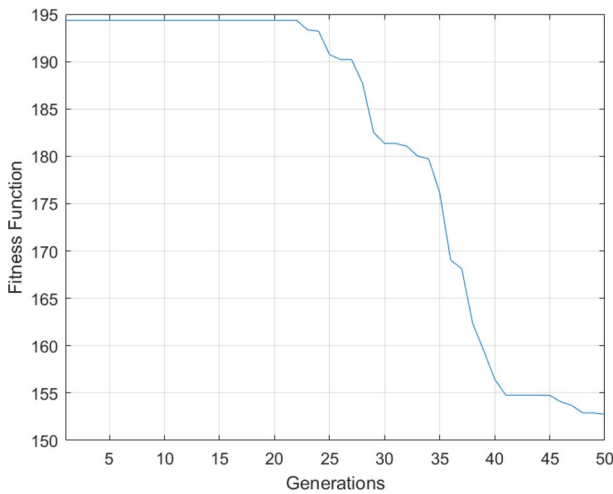


Fig. 9 Fitness function evolution—deterministic design

**Table 4** Designed parameters for MB-PSS (deterministic approach—central frequencies)

Generator	$F_L$ (Hz)	$F_I$ (Hz)	$F_H$ (Hz)
01	0.040052	0.54593	6.6796
02	0.090422	0.83242	9.9667
03	0.041969	1.00000	9.9230
04	0.100000	0.47130	6.9764

**Table 5** Designed parameters for MB-PSS (deterministic approach—central gains)

Generator	$K_L$ (pu)	$K_I$ (pu)	$K_H$ (pu)	$K_G$ (pu)
01	4.3103	7.0227	16.524	9.5954
02	28.499	1.0395	34.644	6.3234
03	0.0100	2.1117	0.0100	5.8199
04	0.0100	0.0100	16.826	20.0000

**Table 6** Probabilistic analysis of the deterministic design

Parameter	MCS	2PEM
Algorithm	<b>2</b>	<b>3</b>
Samples	5000	28
Computational burden	5.6324 min	2.9503 s
$\mu_{\xi_{\min}}$	9.8799%	9.8983%
$\sigma_{\xi_{\min}}$	0.33253%	0.37486%
$P_r\{\xi_{\min} \geq \xi_d\}$	<b>35.894%</b>	<b>39.31%</b>
$\mu_{\sigma_{\max}}$	-0.17699	-0.17702
$\sigma_{\sigma_{\max}}$	0.00097015	0.00096842
$P_r\{\sigma_{\max} < 0\}$	100%	100%

Bold values are used to highlight the probabilities of security

The closed-loop system with designed controllers (whose parameters are presented in Tables 4 and 5) presents a minimum damping ratio of 10.004% ( $\xi_{\min} = 10.004\%$ ) and a spectral abscissa of  $-0.17698$  ( $\sigma_{\max} = -0.17698$ ).

From a deterministic perspective, the system demonstrates stability in closed-loop operation, as verified by Algorithm 1. However, it is crucial to assess the stability probabilistically. In this approach, the loads are modeled with a mean equivalent to their nominal values and a standard deviation of 5% of these mean values. The comparative results are presented in Table 6. The means and standard deviations derived from the 2PEM are observed to be closely aligned with those obtained by the MCS, but the computational effort required for the 2PEM is substantially lower. Figures 10 and 11 illustrate the convergence pattern of the MCS, indicating the stabilization of results between 2000 and 3000 samples, which is considerably higher than the sample count required for the 2PEM. In particular, the probability of satisfying the security constraint ( $P_r\{\xi_{\min} \geq 10\%\}$ ) with MB-PSS (designed by the deterministic

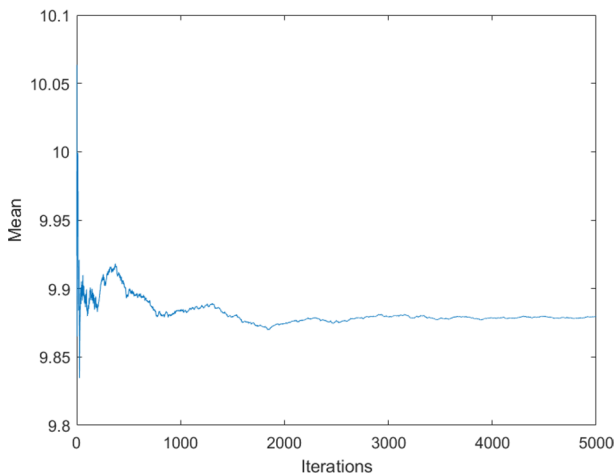


**Fig. 10** Convergence of Monte Carlo simulation ( $\mu_{\xi_{\min}}$ —deterministic design)

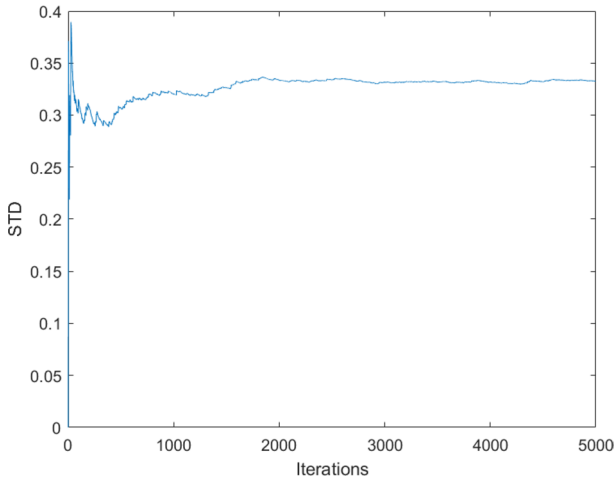


**Fig. 11** Convergence of Monte Carlo Simulation ( $\sigma_{\varepsilon_{\min}}$ —deterministic design)

approach) falls below 40%, significantly lower than the desired confidence level of 95%. This discrepancy underscores the necessity of the proposed approach in this paper for designing robust controllers under uncertainties.

### 4.1.3 Probabilistic design using the proposed approach

The implementation of the proposed approach involved 25 particles and 50 iterations, leading to 1250 fitness evaluations ( $25 \times 50 = 1250$ ). For the design and validation stages, the loads were modeled with means equivalent to their nominal values and a standard deviation of 5% of these mean values. A confidence level of 95% was maintained for security and stability requirements, as delineated in (23)–(24). A minimum damping ratio of 10% was established to ensure security.

**Table 7** Designed parameters for MB-PSS (probabilistic approach—central frequencies)

Generator	$F_L$ (Hz)	$F_I$ (Hz)	$F_H$ (Hz)
01	0.056086	0.92914	10.0000
02	0.038109	1.00000	5.83010
03	0.010000	0.38560	10.0000
04	0.045834	1.00000	8.55430

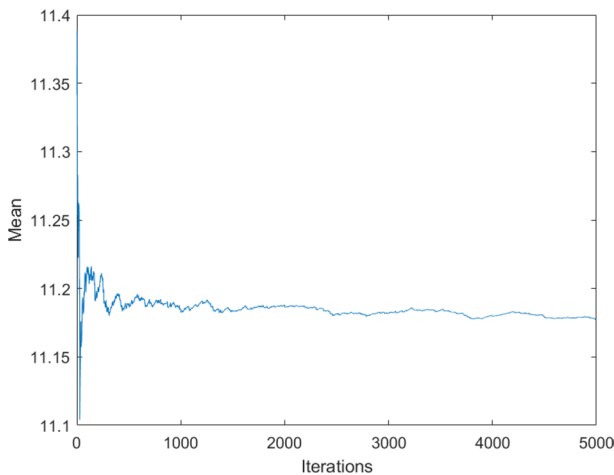
**Table 8** Designed parameters for MB-PSS (probabilistic approach—central gains)

Generator	$K_L$ (pu)	$K_I$ (pu)	$K_H$ (pu)	$K_G$ (pu)
01	0.0100	3.6353	18.513	9.1452
02	9.8333	0.0100	11.597	5.5021
03	10.754	26.511	0.0100	0.79618
04	0.0100	0.0100	37.673	16.5740

**Table 9** Probabilistic analysis of the probabilistic design

Parameter	MCS	2PEM
Algorithm	<b>2</b>	<b>3</b>
Samples	5000	28
Computational burden	5.942 min	3.0857 s
$\mu_{\xi_{\min}}$	11.177%	11.151%
$\sigma_{\xi_{\min}}$	0.40103%	0.69405%
$P_r\{\xi_{\min} \geq \xi_d\}$	<b>99.834%</b>	<b>95.133%</b>
$\mu_{\sigma_{\max}}$	-0.2005	-0.2005
$\sigma_{\sigma_{\max}}$	0.00079291	0.00079124
$P_r\{\sigma_{\max} < 0\}$	100%	100%

Bold values are used to highlight the probabilities of security

**Fig. 12** Convergence of Monte Carlo simulation ( $\mu_{\xi_{\min}}$ —probabilistic design)

The process converged in 21 min. The optimized parameters resulting from this study are detailed in Tables 7 and 8.

To evaluate the efficacy of the results, Algorithms 2 and 3 (both MCS and 2PEM) were carried out, with the main results presented in Table 9. The results of both methods are consistent, and the probability of meeting the security constraint exceeds the required confidence level of 95%. In the MCS analysis, 5000 samples were used, whereas the 2PEM required only 28 samples, a fixed number determined by the count of uncertainty input variables. As noted in the previous section, the MCS stabilized its mean and standard deviation values between 2000 and 3000 samples, as illustrated in Figs. 12 and 13. This sample size is significantly more significant than that required for the 2PEM. It is essential to note that 1500 fitness function evaluations were performed during optimization. The 2PEM (referenced in Algorithm 3) required 28 deterministic modal analyses for each evaluation. In contrast, employing MCS (Algorithm 2) would require

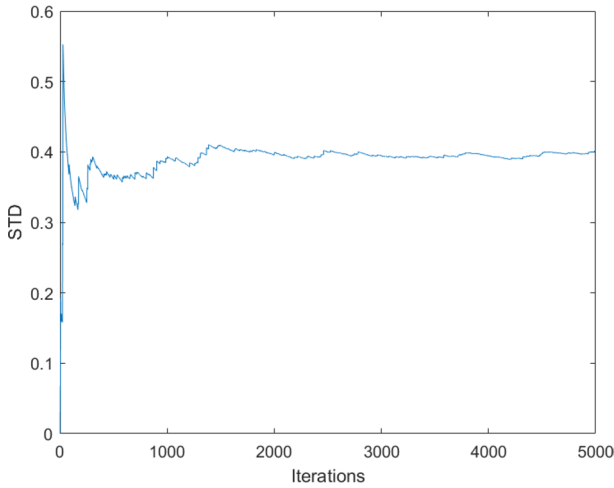


Fig. 13 Convergence of Monte Carlo simulation ( $\sigma_{\xi_{\min}}$ —probabilistic design)

2000 to 3000 samples, underscoring the efficiency of using 2PEM for designing MB-PSS.

Finally, it is important to note that stabilizing the mean and standard deviation of the output variables is a common practice in the literature [57, 62] to ensure the reliability of results obtained by Monte Carlo simulation (MCS). This is because, beyond a certain number of simulations (samples), there is no significant gain in precision for the statistical measures of output variables (mean and standard deviation) as the number of samples increases. Therefore, in this paper, the number of samples used is considered sufficient to ensure the statistical significance of the results.

#### 4.1.4 Impact of the uncertainty level

The previous analyses involved load uncertainties modeled with a standard deviation of 5%. To examine the impact of uncertainties on the tuning carried out (parameters

Table 10 Impact of the loads uncertainty level—2PEM

Standard deviation of loads ( $\sigma_{P_{dk}}, \sigma_{Q_{dk}}$ )	5%	2.5%	10%
$\mu_{\xi_{\min}}$	11.151%	11.263%	10.913%
$\sigma_{\xi_{\min}}$	0.69405%	0.19387%	1.6245%
$P_r\{\xi_{\min} \geq \xi_d\}$	<b>95.133%</b>	<b>100%</b>	<b>71.29%</b>
$\mu_{\sigma_{\max}}$	- 0.2005	- 0.20049	- 0.19865
$\sigma_{\sigma_{\max}}$	0.00079124	0.0003944	0.01011
$P_r\{\sigma_{\max} < 0\}$	100%	100%	100%

Bold vlaues are used to highlight the probabilities of security

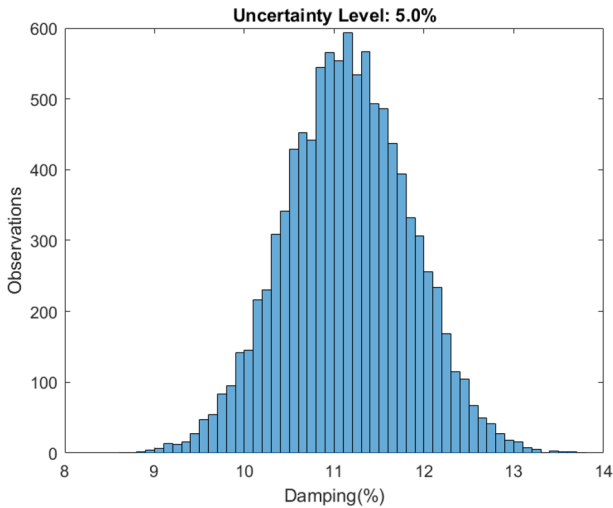


**Fig. 14** Histogram for  $\xi_{\min}$  ( $\sigma_{P_{dk}} = \sigma_{Q_{dk}} = 5.0\%$ )

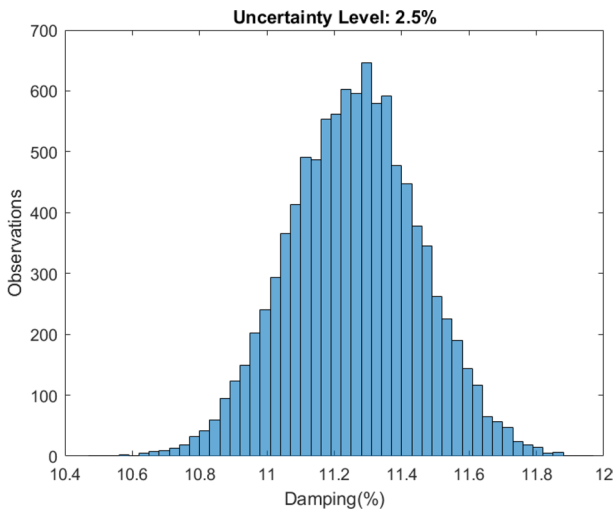


**Fig. 15** Histogram for  $\xi_{\min}$  ( $\sigma_{P_{dk}} = \sigma_{Q_{dk}} = 2.5\%$ )

specified in Tables 7 and 8) Algorithm 3 was applied with varying standard deviations for  $\sigma_{P_{dk}}$  and  $\sigma_{Q_{dk}}$  (2.5% and 10%). The results are summarized in Table 10, showing that the probability of maintaining stability security (negative spectral abscissa) consistently remains 100%. However, the uncertainty level in the loads influences the probability of meeting the security requirement (minimum damping ratio of 10%). For a standard deviation equal to 2.5%, less than the value used in the tuning stage, the probability increases to 100%. In contrast, increasing the standard deviation to 10% reduces this probability. This trend aligns with the expectation



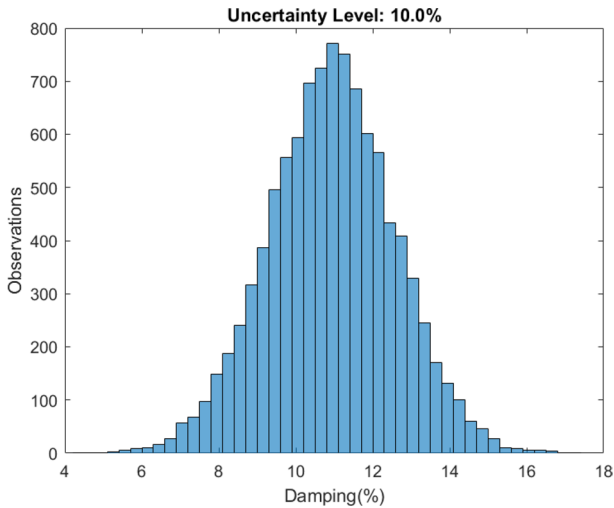


**Fig. 16** Histogram for  $\xi_{\min}$  ( $\sigma_{P_{dk}} = \sigma_{Q_{dk}} = 10.0\%$ )

that higher input uncertainty leads to increased output uncertainty. Figures 14, 15, and 16 showcase histograms of the minimum damping ratio in closed-loop operation for various uncertainty levels. To construct each figure,  $10^4$  samples were generated using the values of  $\mu_{\xi_{\min}}$  and  $\sigma_{\xi_{\min}}$  from Table 10, indicating that higher uncertainty levels lead to greater dispersion of the output variable.

#### 4.1.5 Nonlinear time-domain simulation

The efficacy of the proposed approach, particularly in the context of angular small signal stability, should be further validated through nonlinear time-domain simulations for angular transient stability assessment. In this simulation, a short circuit is introduced in bus 5 for 50 ms, cleared by disconnecting lines 5-1 for another 50 ms, and reclosed. This scenario is tested under the nominal operating conditions specified in Appendix 1. The deterministic and probabilistic tuning approaches (as presented in Tables 4, 5, 7, and 8) are evaluated using Anatem software [63]. The results show internal angles, MB-PSS outputs, and voltage magnitudes in Figures 17, 18, 19, 20 and 21. These figures indicate that the system remains stable post-disturbance, returning to its initial state after restoring the network topology.

#### 4.1.6 Sensitivity analysis

Particle Swarm Optimization has proven to be highly effective in solving the proposed approach in this work. However, as noted in the literature [64], the number of individuals and generations employed significantly influences the quality of its solutions. It is crucial to emphasize that while PSO does not guarantee a global optimal solution, it is capable of providing high-quality solutions in reasonable

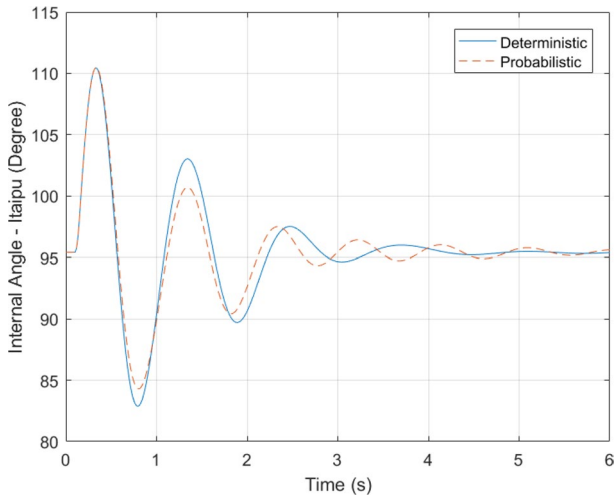


**Fig. 17** Internal angle (Itaipu—Generator 4)

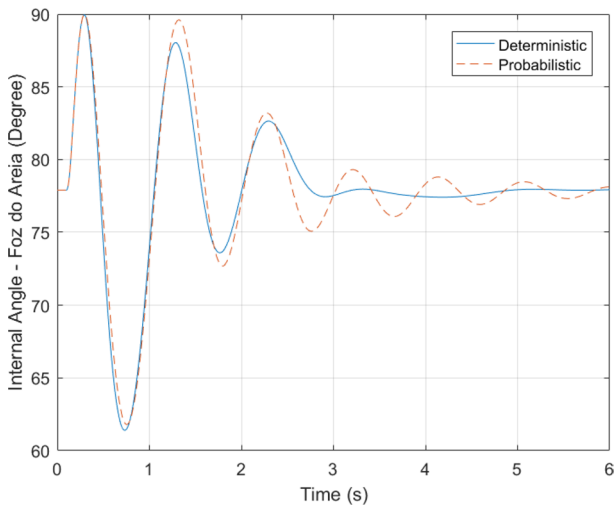


**Fig. 18** Internal angle (Foz do Areia—Generator 3)

computational time. In this section, we present simulations of three different cases, with the results summarized in Table 11 and Fig. 22. For these cases, the number of fitness function evaluations was kept constant (approximately 1250) to maintain a similar computational burden of around 21 min. As shown in Table 11, for this particular problem and system, employing 25 individuals and 50 generations (as used in previous simulations) produced the lowest value of the fitness

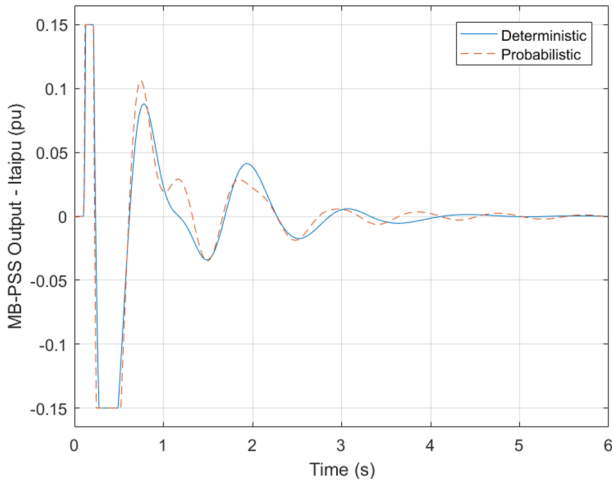


Fig. 19 Itaipu controller output ( $V_{PSS4}$ )

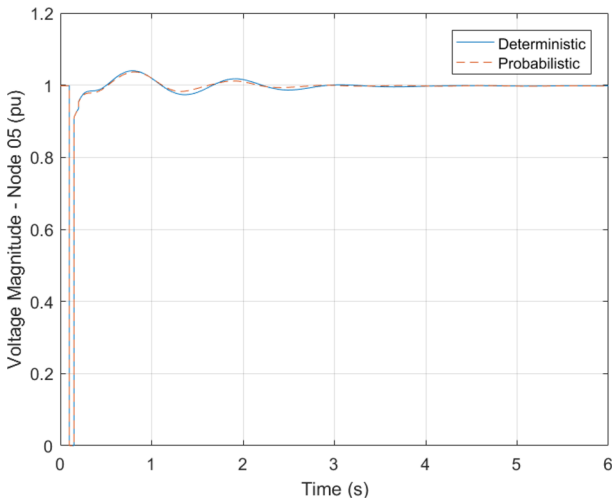


Fig. 20 Voltage magnitude at node 05

function (summation of gains). Figure 22 illustrates the convergence of the fitness function in each simulation.

## 4.2 New England test system

### 4.2.1 System description and simulation scenarios

The New England test system, depicted in Fig. 23, will be used to discuss the results derived from the proposed approach. Comprising 39 nodes and 10 generators, the

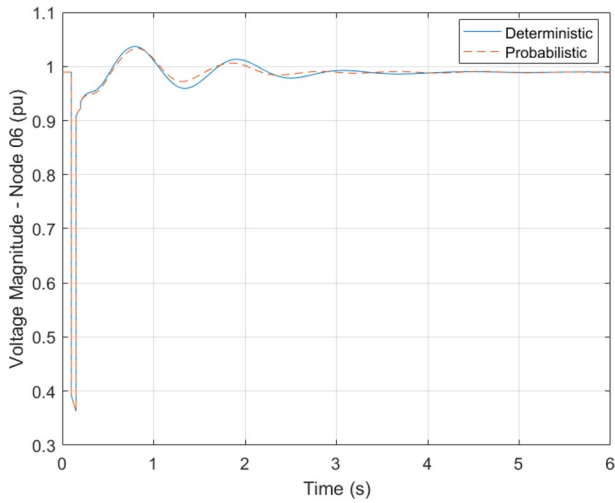


**Fig. 21** Voltage magnitude at node 06

**Table 11** Sensitivity analysis

Simulation	Individuals	Generations	Evaluations	Fitness	Computational burden (min)
01	25	50	1250	150.58	20.9
02	20	63	1260	187.23	21.4
03	50	25	1250	198.86	21.3

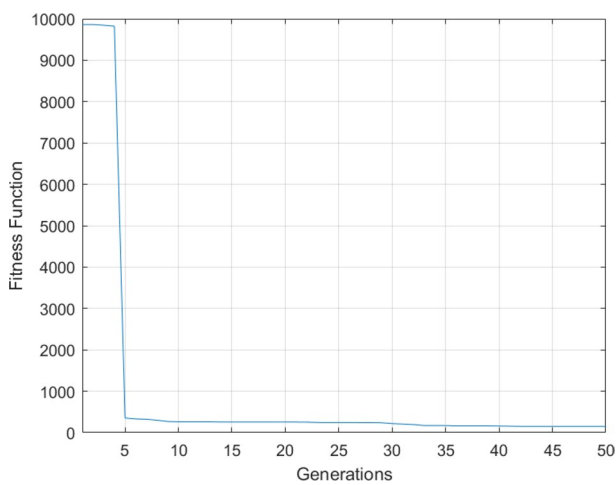


**Fig. 22** Fitness function evolution—probabilistic design

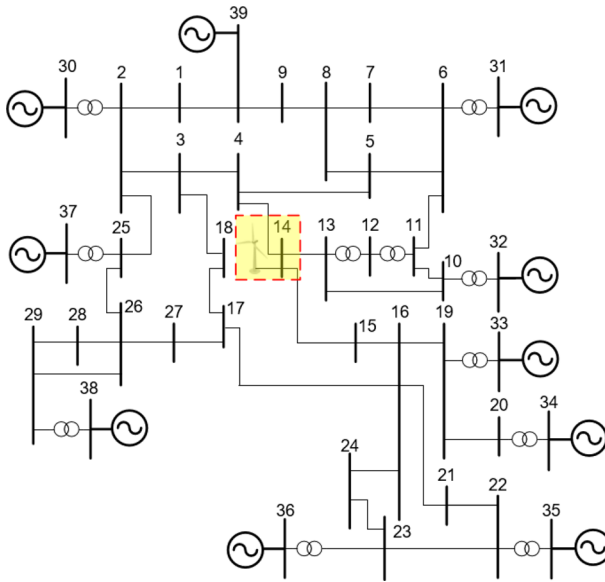


**Fig. 23** New-England test system

detailed data for this system can be accessed in [65]. In the base case, this system has a total load of 6097.1 MW and 1408.9 MVar, with active power generation of 6140.8 MW. In this specific case study, a wind generator with a dispatch capacity of 920 MW is placed at node 14, representing approximately 15% of the active power generation of the base case [66]. The unity power factor is adopted for the wind generator.

The base case is used to design the MB-PSS in this case study. The minimum damping ratio in open loop operation ( $\xi_{\min}$ ), calculated by deterministic analysis, is  $-6.0421\%$ . Therefore, MB-PSS will be integrated into the system. In particular, the generator located at node 39 represents an equivalent system and is thus excluded from receiving a PSS. The same limits presented in Table 3 are considered during the optimal adjustment of MB-PSS.

The following PSO parameters were used for deterministic and probabilistic designs: 25 particles and 50 iterations. This results in 1250 fitness function evaluations ( $25 \times 50 = 1250$ ). For probabilistic assessment and design, loads and wind generation are modeled with a mean equivalent to their nominal values and a standard deviation of 5% of these mean values.

#### 4.2.2 MB-PSS design

The deterministic approach detailed in Appendix 2 and the probabilistic approach outlined in Sect. 3 were applied (which took around 2.5 h to converge). Figure 24 shows the evolution of the fitness function, with optimal fitness values of 798.13 for the probabilistic design and 740.3 for the deterministic approach. The higher value for the probabilistic design is due to the increased control effort required to ensure

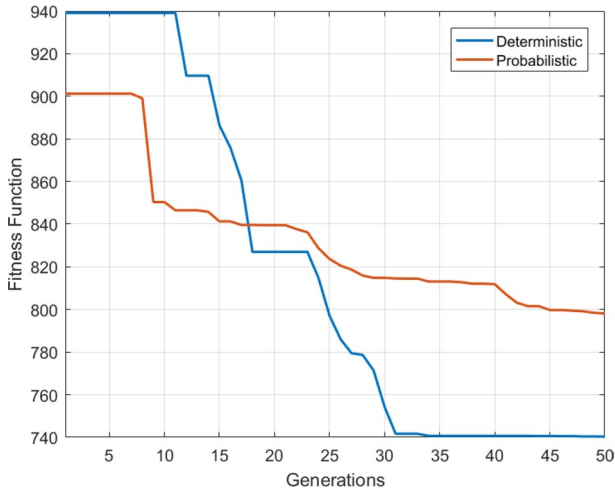


**Fig. 24** Fitness function evolution—New England test system

**Table 12** Designed parameters for MB-PSS (deterministic approach—central frequencies—New England)

Generator	$F_L$ (Hz)	$F_I$ (Hz)	$F_H$ (Hz)
30	0.02874	0.53469	6.4613
31	0.019191	0.96661	4.0490
32	0.085262	0.51747	3.9448
33	0.047169	0.25629	4.2840
34	0.064422	0.27426	3.4189
35	0.098322	0.88478	6.9181
36	0.07895	0.38012	10.0000
37	0.080941	0.52311	3.4329
38	0.042355	0.60414	5.2529

**Table 13** Designed parameters for MB-PSS (deterministic approach—central gains—New England)

Generator	$K_L$ (pu)	$K_I$ (pu)	$K_H$ (pu)	$K_G$ (pu)
30	17.394	0.010	120.000	13.958
31	19.817	6.4876	44.105	9.4976
32	5.3292	2.2012	45.021	4.6594
33	0.010	12.607	49.915	3.0165
34	1.0402	17.810	16.627	8.2441
35	20.682	0.021017	44.005	6.7611
36	0.010	24.437	50.666	9.0492
37	6.4717	16.016	96.185	4.809
38	3.2573	19.762	37.222	3.1986

**Table 14** Designed parameters for MB-PSS (probabilistic approach—central frequencies—New England)

Generator	$F_L$ (Hz)	$F_I$ (Hz)	$F_H$ (Hz)
30	0.035989	0.66537	3.4451
31	0.041553	0.79252	6.4613
32	0.071798	0.55841	4.7447
33	0.060337	0.56664	6.0087
34	0.050435	0.32625	4.6337
35	0.073635	0.48188	6.2160
36	0.040460	0.36701	9.1179
37	0.043975	0.35137	4.4955
38	0.033315	0.87970	4.9708

**Table 15** Designed parameters for MB-PSS (probabilistic approach—central gains—New England)

Generator	$K_L$ (pu)	$K_I$ (pu)	$K_H$ (pu)	$K_G$ (pu)
30	6.9505	4.2155	111.010	11.018
31	12.824	4.0122	50.428	8.919
32	10.373	5.7613	41.807	1.9259
33	6.0361	20.429	57.186	8.3482
34	4.4656	21.885	30.943	6.0644
35	13.589	0.010	50.233	11.337
36	2.0523	22.572	47.612	6.6916
37	16.230	23.629	82.537	3.9466
38	4.899	32.120	54.027	2.0451

**Table 16** Mean and standard deviation of damping ratio (New England)

Deterministic design			Probabilistic design		
$\mu_{\xi_{\min}}$	$\sigma_{\xi_{\min}}$	$P_r\{\xi_{\min} \geq \xi_d\}$	$\mu_{\xi_{\min}}$	$\sigma_{\xi_{\min}}$	$P_r\{\xi_{\min} \geq \xi_d\}$
9.9745	0.063883	34.465	10.202	0.11973	95.433

**Table 17** Mean and standard deviation of spectral abscissa (New England)

Deterministic design			Probabilistic design		
$\mu_{\sigma_{\max}}$	$\sigma_{\sigma_{\max}}$	$P_r\{\sigma_{\max} < 0\}$	$\mu_{\sigma_{\max}}$	$\sigma_{\sigma_{\max}}$	$P_r\{\sigma_{\max} < 0\}$
- 0.11113	0.00031856	100	- 0.18073	0.00072418	100

that the security probability exceeds the required confidence level (95%). Tables 12, 13, 14 and 15 present the MB-PSS parameters considering the deterministic and probabilistic approaches.

### 4.2.3 Probabilistic assessment

The results presented in Sect. 4.2.2 are validated using the two-point estimation method (Algorithm 3). Tables 16 and 17 illustrate that the deterministic design may not ensure safe operation under uncertainties. In contrast, the probabilistic approach matches the required confidence level.

## 4.3 General discussion

The proposed approach can play a crucial role in modern power systems, where stability analysis under uncertainties is essential to ensure secure operation, as discussed in [67]. The first advantage of the proposed approach is its ability to provide multi-band PSS parameters that ensure security and stability under uncertainties. The second advantage is the employment of the Unscented Transformation, which allows for executing probabilistic analysis with a reduced number of samples compared to the Monte Carlo simulation. Finally, the proposed approach is formulated to be solved by any type of metaheuristic, and future work will focus on identifying other metaheuristics that could yield promising results. Another advantage of the proposed methodology is its practical applicability in modern systems, as it is based on the simulation of various deterministic stability analysis cases (which can be performed by software already used in the electric sector, maintaining the various models and components developed over the years).

It is important to emphasize that probabilistic small signal stability analysis requires a significant computational burden compared to the deterministic approach. However, parallel computation can be employed to address this issue, as the evaluation of each sample and each individual is independent of the others.

## 5 Conclusions

The approach proposed in this study for the probabilistic tuning of Multi-Band Power System Stabilizers (MB-PSS) successfully met the desired probabilities for security and stability requirements. Although deterministic tuning demonstrated a low computational demand, the performance of the MB-PSS designed through this method did not satisfy the requirements under uncertain conditions. In contrast, the proposed approach converged in a reasonable computational time and achieved the required confidence level. A comparative analysis between Monte Carlo Simulation (MCS) and the Two-Point Estimate Method (2PEM) revealed that MCS needed between 2000 and 3000 samples to achieve accurate results, whereas 2PEM required only 28 samples (for the Brazilian test system). Moreover, as anticipated, it was observed that the performance of the MB-PSS could deteriorate under high load uncertainty levels, which were not considered during the tuning phase. Finally, time-domain simulations demonstrated that the MB-PSS designed through this approach effectively ensured angular transient stability.



**Table 18** Bus data

Node	Type	V (pu)	Gen (MW)	Load (MW)	Load (MVar)	Shunt (MVar)
01	PV	1.030	1658	2405	- 467	179.2
02	PV	1.030	1332	692.3	- 184	149.1
03	PV	1.029	1540	688.2	- 235	114.2
04	PV	1.039	6500	62.6	24.3	36.8
05	PQ	-	-	845.8	- 9.2	33
06	PQ	-	-	- 4.9	79.8	2142
07	Vθ	0.966	-	2884	- 196	42

**Table 19** Branch data

From	To	Resistance (%)	Reactance (%)
01	03	0.0300	0.3800
02	03	0.0500	0.7600
04	06	0.0290	0.7340
05	01	0.1900	2.4500
05	02	0.1500	2.2500
06	05	0.0000	0.3900
06	07	0.0400	0.5700

**Table 20** Generator data

Gen	$X_d$	$X_q$	$X'_q$	$H$	$D$	$T'_{d0}$	$K_A$	$T_A$
01	0.044737	0.036842	0.0157890	85.50	0	5.0	30	0.05
02	0.060714	0.050000	0.0214290	63.00	0	5.0	30	0.05
03	0.045267	0.035494	0.0154320	87.48	0	5.0	30	0.05
04	0.013569	0.010252	0.0045228	336.29	0	7.6	30	0.05
07	0.016667	0.011667	0.0050000	300.00	0	8.0	30	0.05

## Appendix 1

Tables 18, 19 and 20 present data pertaining to the South-Southeastern Brazilian equivalent system [52, 61]. The base power is set at 100 MVA. Specifically, in Table 20, the reactances are expressed in per unit (pu), time constants are listed in seconds, inertia constants in per unit (pu), and gains are also provided in per unit (pu). The analysis incorporates a static excitation system with constants  $K_A$  and  $T_A$ . A third model represents generators, and the loads follow a constant impedance model in dynamic studies.

For nonlinear time domain simulations in Anatem software [63], the following limits have been considered [25, 59]:

- Excitation systems:  $E_{FD\min} = -5.0\text{pu}$  and  $E_{FD\max} = 6.0\text{pu}$ .
- MB-PSS (see Fig. 2):  $V_{L\max} = -V_{L\min} = 0.075\text{pu}$ ,  $V_{I\max} = -V_{I\min} = 0.60\text{pu}$ ,  $V_{H\max} = -V_{H\min} = 0.60\text{pu}$ , and  $V_{ST\max} = -V_{ST\min} = 0.15\text{pu}$ .

## Appendix 2

Multi-Band Power System Stabilizers can also be designed using the deterministic approach detailed in (50)–(53). This solution utilizes the particle swarm optimization method, applying the Algorithm 1 for deterministic small signal stability analysis. Furthermore, the constraints outlined in (51)–(52) are addressed through penalization, as described in Sect. 3.2.

$$\min f(z) = \sum_{k=1}^{npss} (K_{Lk} + K_{Ik} + K_{Hk} + K_{Gk}) \quad (50)$$

$$\text{s.t. } \xi_{\min} \geq \xi_d \quad (51)$$

$$\sigma_{\max} < 0 \quad (52)$$

$$z_k^{\min} \leq z_k \leq z_k^{\max} \quad (53)$$

**Acknowledgements** The author sincerely thanks INERGE, CAPES, CNPq, and FAPEMIG for their support. He also thanks CEPEL for granting permission to use the academic software versions of ANATEM. Lastly, profound appreciation is expressed for the technical support provided by the Optimization, Control, and Power System Stability Research Group (GOCES) at UFSJ, Brazil.

**Data availability** Data will be provided under request.

## References

1. Rogers, G.: Power System Oscillations. Springer, Boston (2000). <https://doi.org/10.1007/978-1-4615-4561-3>
2. Demello, F., Concordia, C.: Concepts of synchronous machine stability as affected by excitation control. IEEE Trans. Power Apparatus Syst. PAS **88**(4), 316–329 (1969). <https://doi.org/10.1109/TPAS.1969.292452>
3. Kundur, P., Klein, M., Rogers, G.J., Zywno, M.S.: Application of power system stabilizers for enhancement of overall system stability. IEEE Trans. Power Syst. **4**(2), 614–626 (1989). <https://doi.org/10.1109/59.193836>
4. Sauer, P.W., Pai, M.A., Chow, J.H.: Power System Dynamics and Stability: With Synchrophasor Measurement and Power System Toolbox 2e. Wiley, Champaign (2017). <https://doi.org/10.1002/9781119355755>
5. Peres, W., De Oliveira, E.J., Passos Filho, J.A., Da Silva Junior, I.C.: Coordinated tuning of power system stabilizers using bio-inspired algorithms. Int. J. Electr. Power Energy Syst. **64**, 419–428 (2015). <https://doi.org/10.1016/j.ijepes.2014.07.040>

6. Dotta, D., e Silva, A.S., Decker, I.C.: Wide-area measurements-based two-level control design considering signal transmission delay. *IEEE Trans. Power Syst.* **24**(1), 208–216 (2009). <https://doi.org/10.1109/TPWRS.2008.2004733>
7. Banerjee, A., Guchhait, P.K., Mukherjee, V., Ghoshal, S.P.: Seeker optimized SVC-PID controller for reactive power control of an isolated hybrid power system. *Energy Syst.* **10**(4), 985–1015 (2019). <https://doi.org/10.1007/s12667-018-0301-0>
8. Zhang, Y., Bose, A.: Design of wide-area damping controllers for interarea oscillations. *IEEE Trans. Power Syst.* **23**(3), 1136–1143 (2008). <https://doi.org/10.1109/TPWRS.2008.926718>
9. Bento, M.E.C.: A procedure to design wide-area damping controllers for power system oscillations considering promising input-output pairs. *Energy Syst.* **10**(4), 911–940 (2019). <https://doi.org/10.1007/s12667-018-0304-x>
10. Bento, M.E.C.: Design of a wide-area damping controller to tolerate permanent communication failure and time delay uncertainties. *Energy Syst.* **13**(1), 235–264 (2022). <https://doi.org/10.1007/s12667-020-00416-6>
11. Grondin, R., Kamwa, I., Trudel, G., Taborda, J., Lenstroem, R., Gérin-Lajoie, L., Gingras, J.P., Racine, R., Baumberger, H.: The multi-band PSS: a flexible technology designed to meet opening markets. In: *Cigrè 2000*, Paris, pp. 1–12 (2000)
12. Kamwa, I., Grondin, R., Trudel, G.: IEEE PSS2B versus PSS4B: the limits of performance of modern power system stabilizers. *IEEE Trans. Power Syst.* **20**(2), 903–915 (2005). <https://doi.org/10.1109/TPWRS.2005.846197>
13. Peres, W.: Multi-band power oscillation damping controller for power system supported by static VAR compensator. *Electr. Eng.* **101**(3), 943–967 (2019). <https://doi.org/10.1007/s00202-019-00830-9>
14. Bian, X.Y., Geng, Y., Lo, K.L., Fu, Y., Zhou, Q.B.: Coordination of PSSs and SVC damping controller to improve probabilistic small-signal stability of power system with wind farm integration. *IEEE Trans. Power Syst.* **31**(3), 2371–2382 (2016). <https://doi.org/10.1109/TPWRS.2015.2458980>
15. Thang, V.V., Trung, N.H.: Probabilistic optimization of planning and operation of networked microgrids with renewable energy resources considering demand response programs. *Energy Syst.* (2022). <https://doi.org/10.1007/s12667-022-00559-8>
16. Haugen, M., Farahmand, H., Jaehnert, S., Fleten, S.E.: Representation of uncertainty in market models for operational planning and forecasting in renewable power systems: a review. *Energy Syst.* (2023). <https://doi.org/10.1007/s12667-023-00600-4>
17. Singh, V., Moger, T., Jena, D.: Uncertainty handling techniques in power systems: a critical review. *Electr. Power Syst. Res.* **203**, 107633 (2022). <https://doi.org/10.1016/j.epsr.2021.107633>
18. Grondin, R., Kamwa, I., Trudel, G., Gérin-Lajoie, L., Taborda, J.: Modeling and closed-loop validation of a new PSS concept, the multi-band PSS. In: *2003 IEEE Power Engineering Society General Meeting, Conference Proceedings*, vol. 3 (2003). <https://doi.org/10.1109/pes.2003.1267430>
19. Ramirez, J.M., Correa, R.E., Hernández, D.C.: A strategy to simultaneously tune power system stabilizers. *Int. J. Electr. Power Energy Syst.* **43**(1), 818–829 (2012). <https://doi.org/10.1016/j.ijepes.2012.06.025>
20. Khodabakhshian, A., Hemmati, R., Moazzami, M.: Multi-band power system stabilizer design by using CPCE algorithm for multi-machine power system. *Electr. Power Syst. Res.* **101**, 36–48 (2013). <https://doi.org/10.1016/j.epsr.2013.03.011>
21. He, P., Wen, F., Ledwich, G., Xue, Y., Wang, K.: Effects of various power system stabilizers on improving power system dynamic performance. *Int. J. Electr. Power Energy Syst.* **46**(1), 175–183 (2013). <https://doi.org/10.1016/j.ijepes.2012.10.026>
22. Rimorov, D., Kamwa, I., Joós, G.: Model-based tuning approach for multi-band power system stabilisers PSS4B using an improved modal performance index. *IET Gener. Transm. Distrib.* **9**(15), 2135–2143 (2015). <https://doi.org/10.1049/iet-gtd.2014.1176>
23. Rimorov, D., Heniche, A., Kamwa, I., Babaei, S., Stefopolous, G., Fardanesh, B.: Dynamic performance improvement of New York state power grid with multi-functional multi-band power system stabiliser-based wide-area control. *IET Gener. Transm. Distrib.* **11**(18), 4537–4545 (2017). <https://doi.org/10.1049/iet-gtd.2017.0288>
24. Khosravi-Charmi, M., Amraee, T.: Wide area damping of electromechanical low frequency oscillations using phasor measurement data. *Int. J. Electr. Power Energy Syst.* **99**, 183–191 (2018). <https://doi.org/10.1016/j.ijepes.2018.01.014>

25. Peres, W., Silva Júnior, I.C., Passos Filho, J.A.: Gradient based hybrid metaheuristics for robust tuning of power system stabilizers. *Int. J. Electr. Power Energy Syst.* **95**, 47–72 (2018). <https://doi.org/10.1016/j.ijepes.2017.08.014>
26. Wang, D., Ma, N., Wei, M., Liu, Y.: Parameters tuning of power system stabilizer PSS4B using hybrid particle swarm optimization algorithm. *Int. Trans. Electr. Energy Syst.* **28**(9), e2598 (2018). <https://doi.org/10.1002/etep.2598>
27. Obaid, Z.A., Muhssin, M.T., Cipcigan, L.M.: A model reference-based adaptive PSS4B stabilizer for the multi-machines power system. *Electr. Eng.* **102**(1), 349–358 (2020). <https://doi.org/10.1007/s00202-019-00879-6>
28. Peres, W., Coelho, F.C.R., Costa, J.N.N.: A pole placement approach for multi-band power system stabilizer tuning. *Int. Trans. Electr. Energy Syst.* **30**(10), e12548 (2020). <https://doi.org/10.1002/2050-7038.12548>
29. Huang, J., Rimorov, D., Moeini, A., Kamwa, I., Darvishi, A., Fardanesh, B., Babaei, S.: Interconnection-level primary frequency control by MBPSS with wind generation and evaluation of economic impacts. *Int. J. Electr. Power Energy Syst.* **119**, 105867 (2020). <https://doi.org/10.1016/j.ijepes.2020.105867>
30. Peres, W., da Costa, N.N.: Comparing strategies to damp electromechanical oscillations through STATCOM with multi-band controller. *ISA Trans.* **107**, 256–269 (2020). <https://doi.org/10.1016/j.isatra.2020.08.005>
31. Alsakati, A.A., Vaithilingam, C.A., Alnasseir, J., Naidu, K., Rajendran, G.: Transient stability enhancement of grid integrated wind energy using particle swarm optimization based multi-band PSS4C. *IEEE Access* **10**, 20860–20874 (2022). <https://doi.org/10.1109/ACCESS.2022.3151425>
32. Djalal, M.R., Robandi, I., Prakasa, M.A.: Stability enhancement of sulselrbar electricity system using mayfly algorithm based on static var compensator and multi-band power system stabilizer PSS2B. *IEEE Access* **11**, 57319–57340 (2023). <https://doi.org/10.1109/ACCESS.2023.3283598>
33. He, P., Wang, M., Sun, J., Pan, Z., Zhu, Y.: Suppression of low-frequency oscillations in power systems containing wind power using DFIG-PSS4B based on MRAC. *Electr. Eng.* (2023). <https://doi.org/10.1007/s00202-023-01899-z>
34. Masseran-Antunes-Parreiras, T.J., Gomes-Junior, S., Nery Taranto, G.: Damping nomogram method for small-signal security assessment of power systems. *IEEE Latin Am. Trans.* **15**(5), 877–883 (2017). <https://doi.org/10.1109/TLA.2017.7910201>
35. Roald, L.A., Pozo, D., Papavasiliou, A., Molzahn, D.K., Kazempour, J., Conejo, A.: Power systems optimization under uncertainty: a review of methods and applications. *Electr. Power Syst. Res.* **214**, 108725 (2023). <https://doi.org/10.1016/j.epsr.2022.108725>
36. Huang, H., Chung, C.Y., Chan, K.W., Chen, H.: Quasi-Monte Carlo based probabilistic small signal stability analysis for power systems with plug-in electric vehicle and wind power integration. *IEEE Trans. Power Syst.* **28**(3), 3335–3343 (2013). <https://doi.org/10.1109/TPWRS.2013.2254505>
37. Ahmadi, H., Seifi, H.: Probabilistic tuning of power system stabilizers considering the wind farm generation uncertainty. *Int. J. Electr. Power Energy Syst.* **63**, 565–576 (2014). <https://doi.org/10.1016/j.ijepes.2014.06.036>
38. Chabane, Y., Ladjici, A.A., Hellal, A., Dookhitram, K.: Cooperative coevolutionary algorithms for optimal PSS tuning based on Monte-Carlo probabilistic small-signal stability assessment. *Int. Trans. Electr. Energy Syst.* **30**(11), e12618 (2020). <https://doi.org/10.1002/2050-7038.12618>
39. Ke, D., Chung, C.Y.: Design of probabilistically-robust wide-area power system stabilizers to suppress inter-area oscillations of wind integrated power systems. *IEEE Trans. Power Syst.* **31**(6), 4297–4309 (2016). <https://doi.org/10.1109/TPWRS.2016.2514520>
40. Wang, Z., Chung, C.Y., Wong, K.P., Tse, C.T.: Robust power system stabiliser design under multi-operating conditions using differential evolution. *IET Gener. Transm. Distrib.* **2**(5), 690 (2008). <https://doi.org/10.1049/iet-gtd:20070449>
41. Gurung, S., Jurado, F., Naetiladdanon, S., Sangswang, A.: Optimized tuning of power oscillation damping controllers using probabilistic approach to enhance small-signal stability considering stochastic time delay. *Electr. Eng.* **101**(3), 969–982 (2019). <https://doi.org/10.1007/s00202-019-00833-6>
42. Gurung, S., Jurado, F., Naetiladdanon, S., Sangswang, A.: Comparative analysis of probabilistic and deterministic approach to tune the power system stabilizers using the directional bat algorithm to improve system small-signal stability. *Electr. Power Syst. Res.* **181**, 106176 (2020). <https://doi.org/10.1016/j.epsr.2019.106176>

43. Gurung, S., Naetiladdanon, S., Sangswang, A.: Coordination of power-system stabilizers and battery energy-storage system controllers to improve probabilistic small-signal stability considering integration of renewable-energy resources. *Appl. Sci. (Switzerland)* **9**(6), 106176 (2019). <https://doi.org/10.3390/app9061109>
44. Gurung, S., Naetiladdanon, S., Sangswang, A.: A surrogate based computationally efficient method to coordinate damping controllers for enhancement of probabilistic small-signal stability. *IEEE Access* **9**, 32822–32896 (2021). <https://doi.org/10.1109/ACCESS.2021.3060502>
45. Hong, H.P.: An efficient point estimate method for probabilistic analysis. *Reliab. Eng. Syst. Saf.* **59**, 261–267 (1998)
46. Yi, H., Hou, Y., Cheng, S., Zhou, H., Chen, G.: Power system probabilistic small signal stability analysis using two point estimation method. In: *UPEC 2007*, pp. 402–407 (2007)
47. Soleimanpour, N., Mohammadi, M.: Probabilistic small signal stability analysis considering wind energy. In: *Iranian Conference on Smart Grids*, pp. 1–6 (2012)
48. Morshed, M.J., Fekih, A.: A probabilistic robust coordinated approach to stabilize power oscillations in DFIG-based power systems. *IEEE Trans. Ind. Inform.* **15**(10), 5599–5612 (2019). <https://doi.org/10.1109/TII.2019.2901935>
49. Fatah Mochamad, R., Preece, R., Hasan, K.N.: Probabilistic multi-stability operational boundaries in power systems with high penetration of power electronics. *Int. J. Electr. Power Energy Syst.* **135**, 107382 (2022). <https://doi.org/10.1016/j.ijepes.2021.107382>
50. Cao, R., Xing, J., Li, Z., Ma, H.: Probabilistic small signal stability analysis with wind power based on maximum entropy theory. *Electr. Power Compon. Syst.* (2024). <https://doi.org/10.1080/15325008.2024.2310775>
51. Eberhart, R., Kennedy, J.: New optimizer using particle swarm theory. In: *Proceedings of the international symposium on micro machine and human science* (1995). <https://doi.org/10.1109/mhs.1995.494215>
52. Canizares, C.: Benchmark models for the analysis and control of small-signal oscillatory dynamics in power systems. *IEEE Trans. Power Syst.* **32**(1), 715–722 (2017). <https://doi.org/10.1109/TPWRS.2016.2561263>
53. Kundur, P.: *Power System Stability and Control*, 1st edn. McGraw-Hill, Nova Iorque (1994)
54. Dill, G.K., e Silva, A.S.: Robust design of power system controllers based on optimization of pseudospectral functions. *IEEE Trans. Power Syst.* **28**(2), 1756–1765 (2013). <https://doi.org/10.1109/TPWRS.2012.2226251>
55. Stott, B.: Review of load-flow calculation methods. *Proc. IEEE* **62**(7), 916–929 (1974). <https://doi.org/10.1109/PROC.1974.9544>
56. Morales, J.M., Pérez-Ruiz, J.: Point estimate schemes to solve the probabilistic power flow. *IEEE Trans. Power Syst.* **22**(4), 1594–1601 (2007). <https://doi.org/10.1109/TPWRS.2007.907515>
57. Verbic, G., Cañizares, C.A.: Probabilistic optimal power flow in electricity markets based on a two-point estimate method. *IEEE Trans. Power Syst.* **21**(4), 1883–1893 (2006). <https://doi.org/10.1109/TPWRS.2006.881146>
58. Morales, J.M., Baringo, L., Conejo, A.J., Mínguez, R.: Probabilistic power flow with correlated wind sources. *IET Gener. Transm. Distrib.* **4**(5), 641–651 (2010). <https://doi.org/10.1049/iet-gtd.2009.0639>
59. IEEE Power Engineering Society: *IEEE Recommended Practice for Excitation System Models for Power System Stability Studies* (IEEE Std 421.5-2005). Energy Development and Power Generating Committee (2005)
60. Montgomery, D.C., Runger, G.C.: Applied statistics and probability for engineers. *Eur. J. Eng. Educ.* **19**(3), 516–517 (1994). <https://doi.org/10.1080/03043799408928333>
61. Boukarim, G.E., Wang, S., Chow, J.H., Tarante, G.N., Martins, N.: A comparison of classical, robust, and decentralized control designs for multiple power system stabilizers. *IEEE Trans. Power Syst.* **15**(4), 1287–1292 (2000). <https://doi.org/10.1109/59.898103>
62. Aien, M., Fotuhi-Firuzabad, M., Aminifar, F.: Probabilistic load flow in correlated uncertain environment using unscented transformation. *IEEE Trans. Power Syst.* **27**(4), 2233–2241 (2012). <https://doi.org/10.1109/TPWRS.2012.2191804>
63. CEPEL: *Anatem User's Manual Version 12.0*. Technical report, Rio de Janeiro (2021). <http://www.dre.cepel.br/>

64. Wang, D., Tan, D., Liu, L.: Particle swarm optimization algorithm: an overview. *Soft Comput.* **22**(2), 387–408 (2018). <https://doi.org/10.1007/s00500-016-2474-6>
65. Peres, W., Passos-Filho, J.A., Coelho, F.C.R., Poubel, R.P.B., Costa, J.N.N.: Dynamic transmission capability calculation using bioinspired optimization. *Int. J. Electr. Power Energy Syst.* **133**, 107227 (2021). <https://doi.org/10.1016/j.ijepes.2021.107227>
66. Tavela, F.M., Filho, J.A.P., Avila, O.F.: Assessment of the impact of wind generation intermittency on electric power systems through security regions. *J. Control Autom. Electr. Syst.* **33**(3), 982–997 (2022). <https://doi.org/10.1007/s40313-021-00870-2>
67. Rafique, Z., Khalid, H.M., Muyeen, S.M., Kamwa, I.: Bibliographic review on power system oscillations damping: an era of conventional grids and renewable energy integration. *Int. J. Electr. Power Energy Syst.* **136**, 107556 (2022). <https://doi.org/10.1016/j.ijepes.2021.107556>

**Publisher's Note** Springer Nature remains neutral with regard to jurisdictional claims in published maps and institutional affiliations.

Springer Nature or its licensor (e.g. a society or other partner) holds exclusive rights to this article under a publishing agreement with the author(s) or other rightsholder(s); author self-archiving of the accepted manuscript version of this article is solely governed by the terms of such publishing agreement and applicable law.